IMPACTS OF THERMAL REDUCTION IN TRANSCEIVER PERFORMANCE ON OUTDOOR SENSING NETWORKS

by

Kenneth Bannister

A Thesis Presented in Partial Fulfillment
of the Requirements for the Degree
Master of Science

ARIZONA STATE UNIVERSITY

May 2009

IMPACTS OF THERMAL REDUCTION IN TRANSCEIVER PERFORMANCE ON OUTDOOR SENSING NETWORKS

by

Kenneth Bannister

has been approved

April 2009

Graduate Supervisory Committee:

Sandeep Gupta, Chair
K. Selçuk Candan
Violet R. Syrotiuk

ACCEPTED BY THE GRADUATE COLLEGE

ABSTRACT

Observations of low-power wireless network links outdoors revealed significant loss in received signal strength (RSS) with increasing temperatures. The primary research goals were to quantify this finding and study the impact on transmission range and reliability of environmental data collection. Experiments measured a linearly increasing loss in RSS to a maximum of 7 dB from 20 degrees Celsius to 60 degrees Celsius, and reduction in maximum communication range of 26 percent in open outdoor conditions. Simulation of multihop data collection showed the maximum RSS reduction halved node connectivity and doubled estimated transmission count (ETX). A secondary research goal was to understand the source of the signal strength loss. Modeling of the transceiver components identified reduction of amplifier gain as a likely source. A network deployment should strive to reduce enclosure temperature swings or compensate for range loss with hardware/software.

ACKNOWLEDGMENTS

I would like to thank my advisor, Sandeep Gupta, for his guidance and support for my research and studies. I also appreciate the service of the other committee members, Profs. Candan and Syrotiuk. I'm grateful to my labmate Gianni Giorgetti for sharing his experience with electronics, wireless, and academic papers.

Resources for experimental work were provided by the Impact Lab at Arizona State, and made possible by awards 0831544 and 0834797 from the National Science Foundation. Thanks also go to the Desert Botanical Garden for providing a location for the sensor network, and the University of Arizona's Maricopa Agricultural Center for use of the field for the communication range experiment.

The constant support and encouragement of my wife Julie was the foundation on which this work was built. I can't thank her enough.

TABLE OF CONTENTS

Page

LIST OF TABLES

LIST OF FIGURES

Figure Page

CHAPTER 1

Introduction to Sensing Networks

Environmental sensing encompasses a broad variety of techniques to measure and report on physical parameters, from a mechanical river level gauge that is recorded manually to an electronic room temperature sensor that provides an automated alert. In this thesis interest is focused on the use of electronic or electromechanical devices embedded outdoors to measure environmental parameters and transmit the data to a base station. Examples of these device systems include the regional *Snowpack Telemetry* (SNOTEL) network of 700 stations across the western United States [37] as well as a small network of ten soil sensors on two hectares of a vineyard [14].

The history of this form of environmental sensing dates back at least to the 1940s with the introduction of an automated weather station that reported readings via radio [42]. In the 1960s the *Sound Surveillance System* (SOSUS), a deep water, cabled hydrophone network for submarine detection became operational [41]. Around 1980 the *Remote Automated Weather Stations* (RAWS) network for fire weather monitoring began, and now includes 2200 stations nationwide that transmit via landline or satellite [38].

Historically the costs, complexity and power requirements of realtime data transmission have been prohibitive for many projects, especially in remote locations. Instead environmental sensing projects have recorded readings locally with a data logger and then periodically connected to that unit on-site to retrieve the information, or they have used manual measurements or recording [13], [27].

1. Low Power Wireless Sensing Networks

In the late 1990s low power *wireless sensor networks* (WSNs) were developed that provide low cost, small scale monitoring, data transmission, and device control [3], [5]. The fundamental components of the network are small, low cost, wireless computing devices known as “motes” that consist of a microcontroller with a few kilobytes of *random access memory* (RAM), a low-power

radio operating in an *Industrial, Scientific, and Medical* (ISM) band, sensors of various kinds, and a small power source, often a pair of AA batteries [39]. Typically the operational architecture of these applications also includes two levels above the motes: 1) a higher-powered intermediate gateway on-site that collects and forwards mote readings via wired or wireless[1] links to 2) a conventional server for long-term storage and access [9]. These characteristics have enabled WSN deployments for a range of purposes that include environmental sensing as well as industrial process sensing and control, target localization and commercial building automation.

The advantages of modern WSNs for environmental sensing have been enthusiastically received. In particular the small scale and high frequency of readings they enable have facilitated studies that were not practical with earlier techniques [11]. Applications include measurement of infrared energy for bird nesting habits [22], microclimate at various heights on a single redwood tree [36], and recording acoustic waves around a volcano for tectonic activity [40].

2. Challenges in an Outdoor Environment

The physical environment imposes a number of challenges for low power WSNs. At the physical level, the electronics must be enclosed for protection from water, wind-blown material, and animals. For example in one study the enclosure for soil moisture motes grounded in a livestock pasture used a flexible design that allowed the structure to bend over completely and then spring back to its original position [24].

Radio communication at ISM band frequencies presents another class of challenges. At these frequencies (typically 900 MHz and 2.4 GHz) radio waves propagate best by line of sight, so obstructions like foliage may severely attenuate the signal. In one experiment a mote with a 90 m nominal range was reduced to 35 m by dense foliage; however a strong directional antenna was able to increase the range to 60 m [28]. Directional antennas are not a panacea though; the more focused

[1] for example, 802.11 or *General Packet Radio Service* (GPRS)

beam requires more precise positioning. One study found significant outages due to the physical effect of wind shaking the antenna and snow buildup even on a low wind-load antenna [19].

The use of WSNs has spread to locales with extreme environmental conditions, which pose extra difficulties for low power motes. For example standard alkaline battery capacity decreases quickly with low temperatures. At a 25mA discharge rate, certain cells that have 2500 mAh capacity at 0°C are reduced to 500 mAh capacity at -20°C [10]. In another example the GlacsWeb project embedded motes within a glacier. To achieve 100 m communication range though the ice required a transmission power increase from the standard 1 mW (0 dBm) to 100 mW (20 dBm) [23]. In the present study we describe how mote performance is affected by another extreme environment, the Sonoran Desert of south-central Arizona, where daily summertime temperatures in an exposed enclosure may vary daily from 20°C to 60°C.

3. Thesis Contributions and Outline

This thesis explores the significantly reduced performance of mote-based low power transceivers outdoors at high temperatures, including signal strength and communication range, and the resulting consequences for multihop data collection. Secondarily we look inside the transceiver itself to understand how temperature alters signal power, including *received signal strength* (RSS) measurement. Below are the main contributions and links to the rest of the work.

We identify an increase in hardware temperature as the source of the decrease in signal strength for a low power transceiver. For example in one experiment we set up two sets of three TelosB-class motes outdoors to exchange sample data for a 24-hour period, while enclosure temperatures varied from 20°C to 60°C. Figure 1(a) shows the RSS values measured by a single receiver for packets sent by the three opposite transmitters. Overall a linear model emerged, with a mean decrease in RSS of 7.2 dB over the 40°C range. Chapter 3 contains details of this work.

We show the significance of the consequent reduction in connectivity and performance for

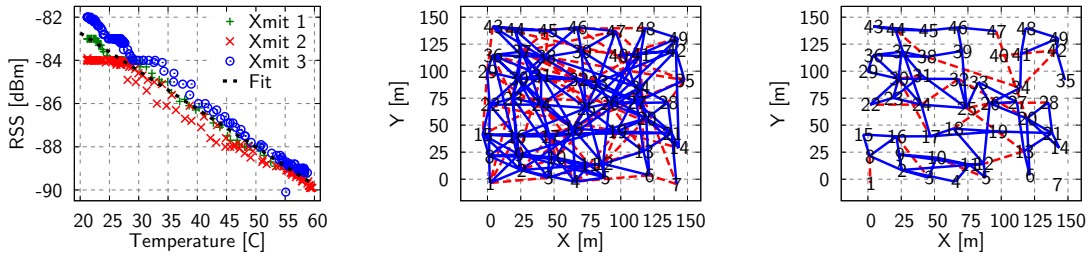

(a) RSS against temperature for received packets, including linear fit.

(b) Mean stats at 20°C: Node connectivity 6.4/8.5 ; ETX 2.8/2.7 for 0.99+/0.4+ PRR.

(c) Mean stats at 60°C: Node connectivity 3.0/3.8, Hop count to sink NA/5.4 for 0.99+/0.4+ PRR; Node 1 link $<$ 1.0 PRR.

Figure 1. Snapshots of key results: a) Signal strength measured outdoors over a 24-hour period; b-c) Connectivity maps of a 7x7 node multihop data collection simulation, where Node 1 at bottom left is the sink node. Solid lines show reliable connectivity near 1.0 PRR, dashed lines show additional marginal connectivity of at least 0.4 PRR.

a simulated environmental sensing network that forwards data towards a single sink. Figure 1(b,c) shows connectivity maps at 20°C and 60°C for a representative trial. At 20°C nodes are well-connected; however by 60°C node connectivity has decreased by more than half. In addition, the *estimated transmission count* (ETX) to the sink has doubled from 2.7 to 5.4, which increases network energy usage and latency of message delivery. Also at 60°C in this example the quality of the sole link to the sink node has become marginal, less than 1.0 *packet reception rate* (PRR). Chapter 4 provides details of the simulation.

Other contributions include experimental confirmation of the expected decrease in maximum communication range for a single link. We found a 26% decrease in an open outdoor environment, near the magnitude predicted by the relevant path loss model. The experiment is described in Chapter 4. Also, we provide transceiver-level interpretation of our experimental results that identify a decrease in amplifier gain as a significant source of the decrease in RSS, based on a two port linear model for signal and noise flow through the transceiver components. This analysis is found in Chapter 5.

CHAPTER 2

Background and Related Work

This chapter describes the network deployment where we first observed a decrease in signal strength with temperature. Then we identify other studies in the literature related to the effect of temperature on low power wireless links.

1. Botanical Garden Sensor Network

We are building a sensor network to measure soil conditions at the Desert Botanical Garden in Phoenix. A wireless mote is connected by a custom-built interface to a soil probe that measures moisture, temperature, and electrical conductivity. Figure 2 shows the system architecture; Figure 3 shows an installed enclosure containing the hardware, the soil probe, and an example of temperature readings from the probe and enclosure. A detailed description of the interface circuitry is provided in Appendix A. The project web page includes graphs of all readings to date and other reports [18].

Hardware performance in general was a particular concern for this network given the extreme summertime conditions in south-central Arizona. We ensured device specifications nominally supported the expected conditions and then verified their operation when stressed. For example our network uses the Moteiv Tmote Sky wireless mote, which supports operating conditions within the industrial range of -40°C to 85°C [25]. However, operational tests found that *universal asynchronous receiver/transmitter* (UART) communication between the mote and the soil probe often failed on winter nights when using the microcontroller's *digitally controlled oscillator* (DCO) to time the data transfer rate. Switching the timer source to the mote's crystal provided reliable results.

Wireless connectivity was another hardware-dependent concern. Figure 4 schematically depicts factors affecting wireless signal strength outdoors. Strength decreases with distance (d in the figure) in a manner specific to the environment. In general an increase in antenna height (h) decreases the rate of strength decrease with distance. Antennas (a) are available with varying strength

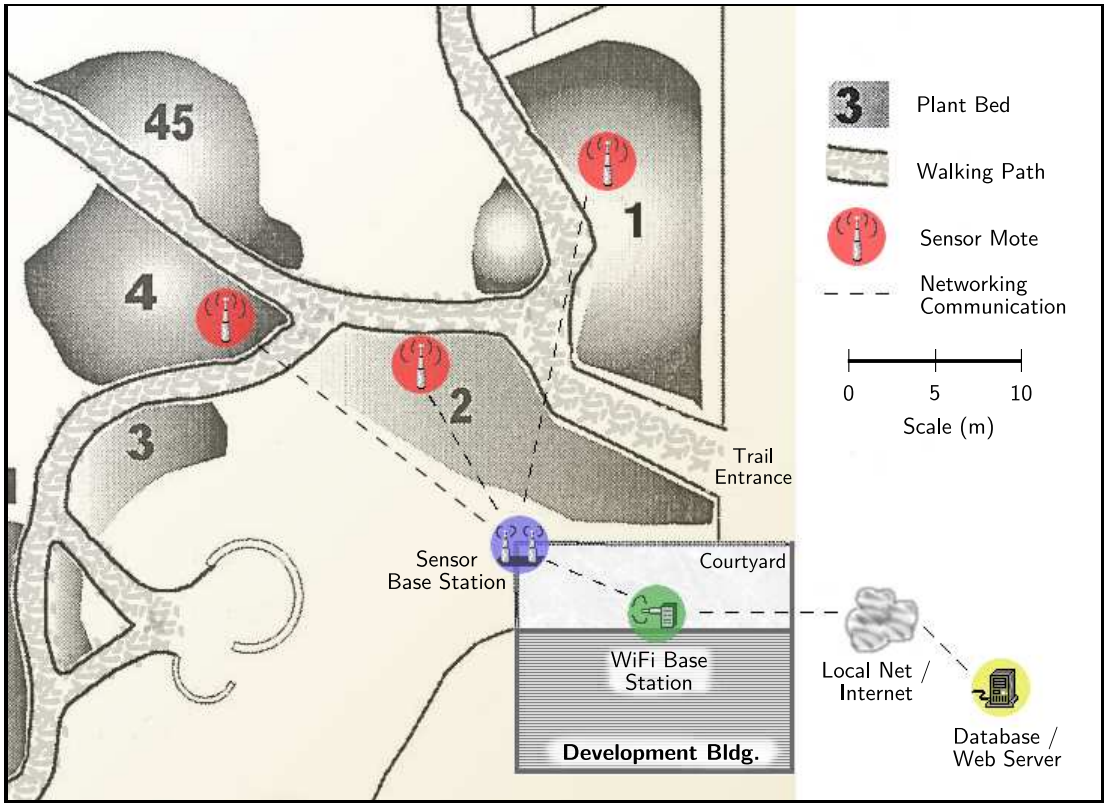

Figure 2. Architecture of sensor network for soil conditions at the Desert Botanical Garden.

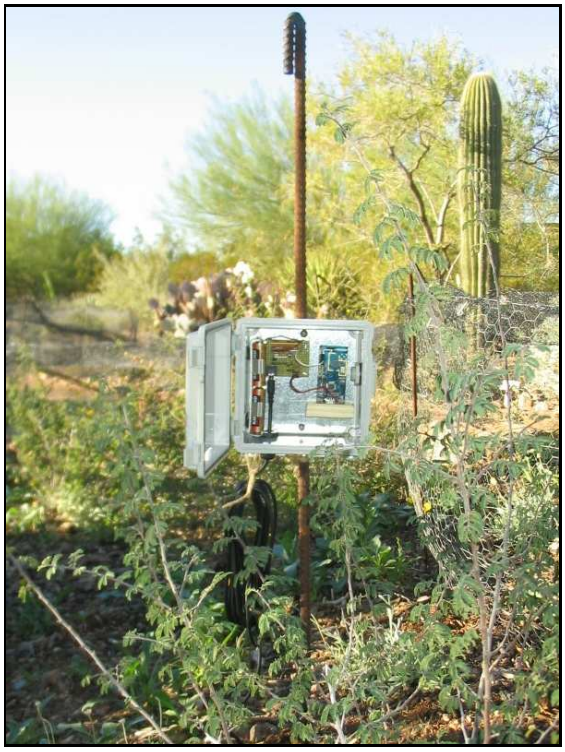

(a) Enclosure containing a Tmote wireless module and probe interface circuitry, installed in Bed 2.

(b) Soil probe inserted at approximately 25 cm (9-10 in) depth.

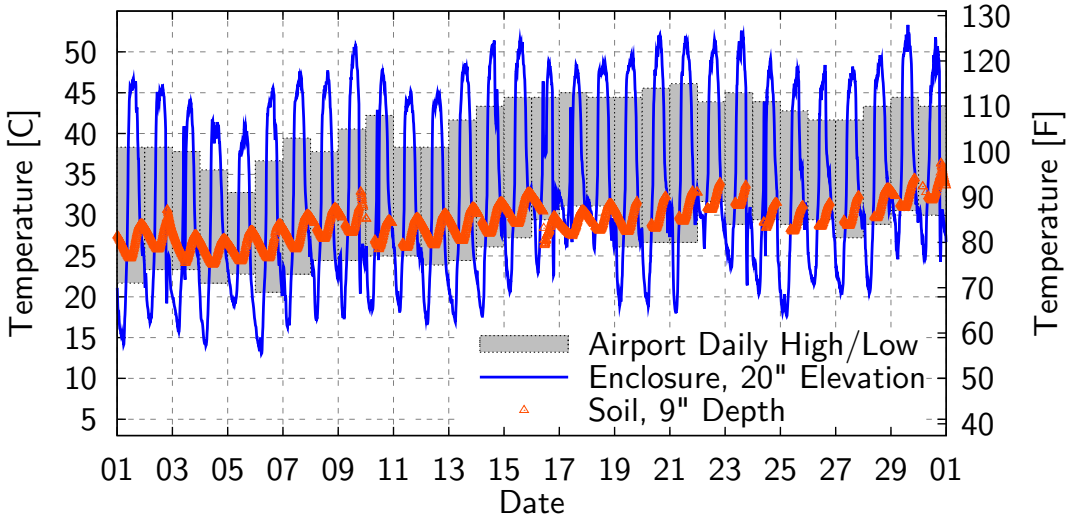

(c) Soil, enclosure and air temperature for June 2008. Enclosure temperatures range approximately 35°C on 6/20-21.

Figure 3. Mote hardware installed at the botanical garden, and sample readings.

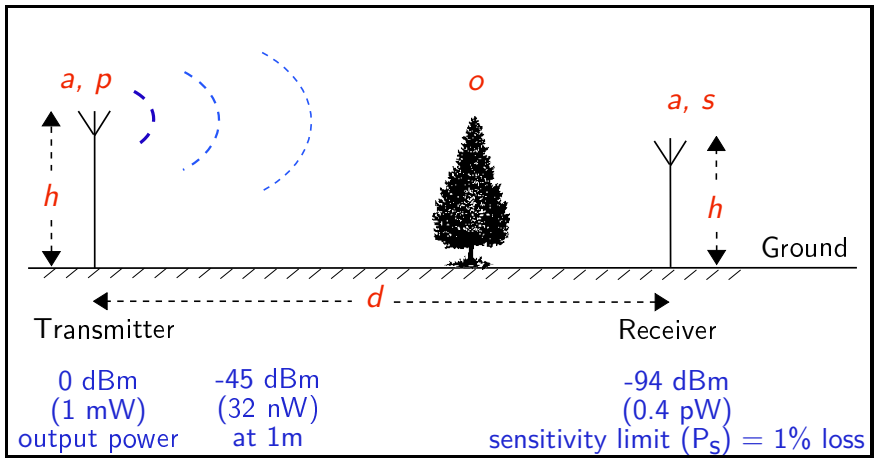

Figure 4. Factors affecting wireless signal strength outdoors: *a* antenna, *d* distance, *h* height, *o* obstructions, *p* output power, and *s* receiver sensitivity. Typical strength levels for low-power transceivers at bottom.

levels and beam directionality, from omnidirectional to tightly focused, to improve both transmission at the sender and reception at the receiver. Output power level (*p*) for a given transmission may be programmed to a range of values. Receiver sensitivity P_s (*s*) is defined as the maximum power level P_r at which the receiver begins to experience packet loss.[1] Greater sensitivity permits detection of fainter signals. Finally, obstructions (*o*) may reduce signal strength by scattering the signal. Figure 4 also shows power levels specific to the Tmote module: maximum output power of 0 dBm and receiver sensitivity of -94 dBm. The dBm scale measures signal strength logarithmically, where a decrease of 3 dBm corresponds to a decrease in power of one-half the original level.

For the botanical garden network, the system architecture map shows the maximum extent of the study area from the base station is approximately 35 meters. Vegetation is mostly low and herbaceous with some shrubs. Short-term communication tests showed that a mote could transmit to the base station across this distance. However given the hot summertime conditions, a week-long communication test was performed at a nearby site to measure the long-term reliability of radio communication.

[1]For IEEE 802.15.4, which is supported by the Tmote, P_s is based on a packet error rate of 1%.

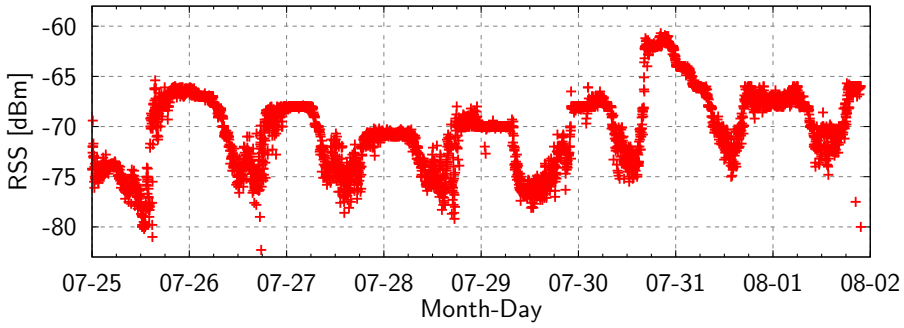

Figure 5. RSS observed for a mote in an outdoor enclosure during a summertime site survey.

2. Observed Variation in Signal Strength

The reliability test found significant daily periodicity in RSS, as shown in Figure 5, often with an amplitude of 7 dB and minima at the hottest time of day. Measured enclosure temperatures ranged from 25°C to 65°C. Neither the data sheet for the Tmote nor its CC2420 transceiver [34] described the effect of temperature on signal strength or transmission range.

A decrease in signal power of this magnitude has important implications for node density in the field. For example if signal strength at a given distance from a transmitter decreases by 7 dB, then in absolute terms the received power is less than one-quarter of the original level. In a free space environment power fades with the square of the distance, so to regain the original power level, the distance to the transmitter must be reduced by more than half.

In a typical outdoor environment the power loss rate with distance is more severe, so a 7 dB drop occurs over a shorter distance than in free space. However in a practical agricultural application, distances of this scale are significant. For example measurement sites may be separated by a distance near the limit of a mote's communication range, and the overall area to be monitored may be measured in hectares, so there is cost pressure to maximize transmission range. Additionally, although a range of 40°C in enclosure temperatures may occur daily only in extreme environments, over the course of a year this range occurs over a much wider area.

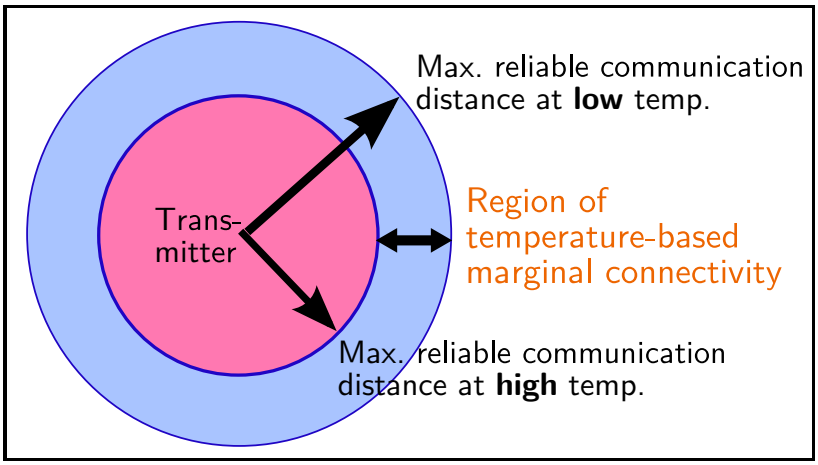

Figure 6. Schematic overhead view of reduction of range with temperature, illustrating the region of marginal connectivity.

Figure 6 conceptually summarizes the main deployment issues raised by the decrease in signal strength with temperature. In particular we seek to quantify the width of the region of marginal connectivity, and estimate the effect on network performance of motes deployed within this region. The significant potential for disrupted communication merits the study of these characteristics and forms the focus of this thesis.

3. Related Work

A survey of the *Wireless Sensor Network* (WSN) literature did not reveal a study that focused on the impact of temperature on link quality. Lin, *et al.* [21] found a daily variation in RSS of around 6 dB outdoors, and Kim, *et al.* [20] also observed RSS variations within *smart containers* outdoors, but neither explored the cause of the variation. Thelen, *et al.* [32] mentioned an inverse relationship between RSS and temperature in a potato field, but focused on humidity. Sun and Cardell-Oliver [31] found that a link may perform better during the day or at night, but suggested humidity or noise was the cause.

In laboratory studies, Yamashita, *et al.* [44] found an approximately 3 dB decrease in output power from 25°C to 65°C in a custom-built module that used the same transceiver as in our work, the

TI CC2420. However that study did not discuss the effect on receiver sensitivity or the implications for networking. The datasheet for the related CC2400 radio shows a decrease in output power of 3 dB and a decrease in sensitivity of 4 dB at 1 Mbps transfer rate over this same temperature range [33].

CHAPTER 3

Signal Strength Measurements and Expected Effects

This chapter describes measurements of the reduction of signal strength with temperature for the Tmote/CC2420 in an initial laboratory study and in more extensive outdoor trials. Then we use well-known path loss models to estimate the consequent reduction in communication range outdoors.

1. Lab Experiment

The goal of this experiment was to measure the effect of temperature on both transmitter output power and receiver input power, and to isolate the effect to the transceiver itself, eliminating variation in the propagation environment. The receiver's RSS was used to measure the signal power. We describe the experimental procedure below in reasonable detail, and provide a full description in Appendix B, including access to the raw data and source code.

Two Tmotes were connected at their antenna input ports by a coaxial cable, as shown schematically in Figure 7. One mote assumed the role of *sender* of test messages, and the other mote was the *receiver* of those messages and measured their RSS. We performed a total of four trials. Relative to the figure, in one trial messages were transmitted left to right and in the second trial from right to left. Then the mote locations were swapped and the two trials were repeated. A cable was used for mote communication rather than wireless to eliminate noise from external sources and signal variability due to multi-path. Attenuators were placed inline to reduce signal power by 60 dB to realistic levels for a production network. The chamber itself was a simple enclosure, and the heat source was a variable-power hot air tool. The mote at room temperature transmitted experimental data in real time to a workstation via *Universal Serial Bus* (USB) connection.

During each trial the sender transmitted a burst of 10 test messages every 40 seconds at the maximum transmission power of 0 dBm. A trial began with the chamber at room temperature and then increased stepwise to 45°C and then 65°C before allowing the mote to cool down. Each

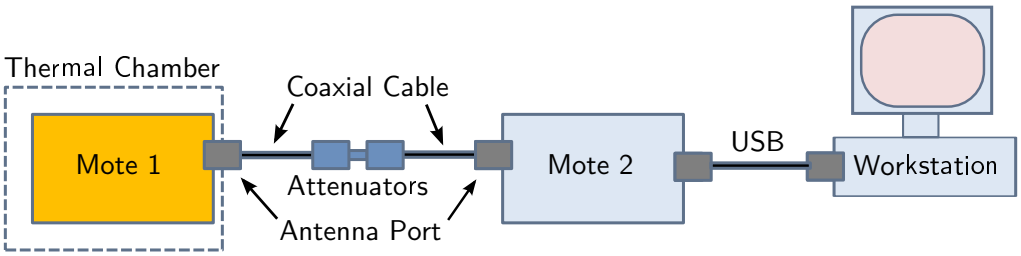

Figure 7. Experimental setup; motes are connected by coaxial cable through *SubMiniature version A* (SMA) connectors at the antenna port.

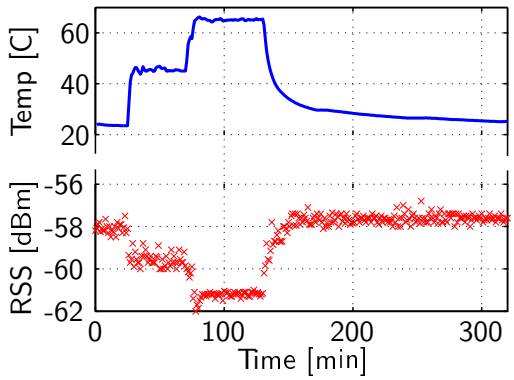

Figure 8. Raw results for a single trial where receiver was heated.

temperature level was maintained for at least 45 minutes to ensure thermal equilibrium with the mote. The mote in the chamber sampled the temperature every 20 seconds, and the temperature level was maintained manually by adjusting the heat source based on observation at the workstation of the temperature readings. Figure 8 illustrates this procedure with the values for temperature and signal strength over time for a single trial where the receiver was heated, and clearly shows an inverse relationship between RSS and temperature.

The mote remaining at room temperature, regardless of its role as transmitter or receiver, was required to forward data for observation to the workstation due to unreliable USB communication at high temperatures. This arrangement meant that when the receiver was heated, it transmitted the temperature and RSS readings *back* to the original sender of the message burst. The timing of this

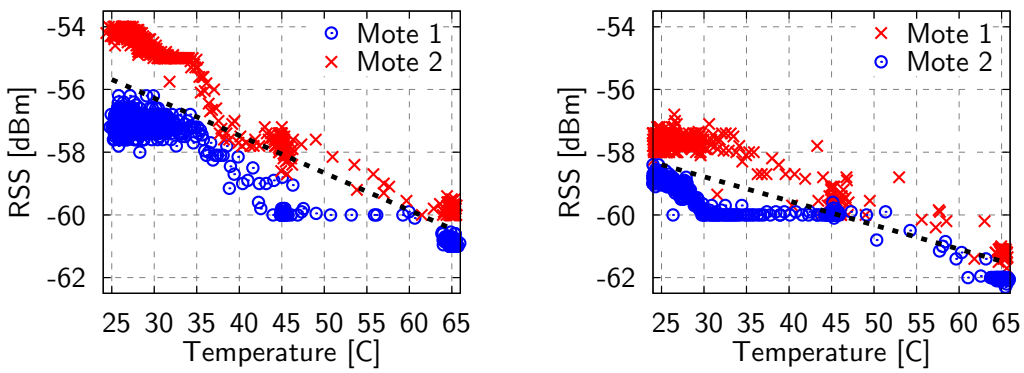

(a) Both trials when only transmitter heated. **(b) Both trials when only receiver heated.**

Figure 9. RSS over temperature, including linear fit, for all trials in the lab.

extra transmission was easily slotted between test message bursts.

Figure 9 shows the linear decrease in RSS graphically. The data appears clumped at 25, 45, and 65°C as the temperature was maintained at these values. Overall transmitter power decreased approximately 5 dB over the 40°C range, and receiver sensitivity decreased approximately 3 dB, for a combined loss of 8 dB, similar to the values in the CC2400 datasheet. We use a linear model to interpolate the data and quantify the power loss at the transmitter and receiver. The equation for the combined *Temperature Loss* ($L_{lab}(T)$) in the lab in dBm is:

$$L_{lab}(T) = 0.200(T - 25), \tag{3.1}$$

where T is the temperature in the range $25°C \leqslant T \leqslant 65°C$.

Significantly, only the motes themselves were heated in the thermal chamber; the coaxial cables remained at room temperature. Therefore we ascribe the loss to the effect of temperature on the motes themselves rather than an effect of the propagation channel.

2. Outdoor Experiment

To confirm the initial laboratory results, we performed more extensive measurements outdoors, our target environment. Six motes were segregated into two groups, α and β, of three motes

each. The motes were located in an open area with the groups separated by about 28 m. Each mote was enclosed in a white plastic bag, which allowed the motes to heat up to approximately 60°C at the hottest part of the day, when ambient air temperature was around 40°C. The motes were elevated approximately 0.5 m above ground, and used the internal inverted-F antenna. A similar setup was used for the experiment pictured in Figure 15 on pg. 25.

Each mote in the α group sent and received packets with each mote in the β group, for a total of nine mote pairs. RSS was averaged over bursts of 100 packets sent at an output power of -10 dBm. The results include only those packet bursts where 100% of packets were received. A cycle of communication included each of the nine mote pairs exchanging a packet burst as both transmitter and receiver. This cycle repeated every nine minutes, and a complete trial ran for approximately 24 hours.

The experiment required substantial coordination between the motes to ensure synchronization and conserve battery power over the full trial period. After mounting a mote, the experiment operator sent several commands to set its output power, communication slot among its siblings, and the length of a communication cycle. Then a separate time beaconing mote was started, which simply broadcast a message containing an integer sequence number every 45 seconds to trigger the start of an exchange between a pair of motes. Each mote used the sequence number and its slot position to initiate a communication session as dictated by the pairings shown in Table 1.

Once a pair of fixed and mobile motes received the time beacon message for their time slot, state transitions for tasks within the slot were time-based as shown in Table 2. There were two timers: *sync-timer* and *state-timer*. Sync-timer managed overall time slot length, and state-timer managed transitions within the slot. If a mote got out of sync with its peers, the sync-timer provided a mechanism to resynchronize.

This communication protocol was tested in the lab over several days before deployment.

Table 1. Communication slots used to pair fixed (F*n*) and movable (M*n*) motes outdoors.

Tick Sequence	1	2	3	4	5	6	7	8	9	10	...
Movable Mote	M1	M2	M3	M2	M3	M1	M3	M1	M2	M1	...
Fixed Mote	F1	F2	F3	F1	F2	F3	F1	F2	F3	F1	...

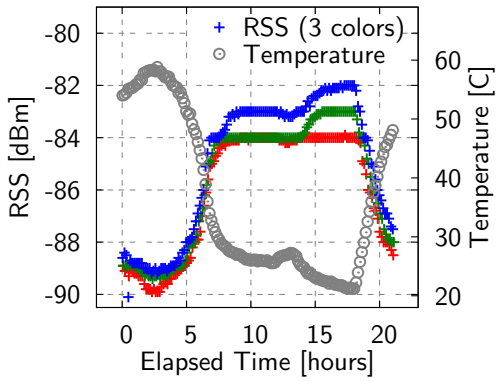

Figure 10. Signal strength and temperature measured by a single receiver from three transmitters outdoors.

Testing revealed that the RSS message burst of 100 packets sometimes required an extra couple of seconds to complete, caused by an unknown phenomenon clearly below the level of the application software. We then incorporated a short time buffer between the tasks in a communication slot to ensure reliability. The final communication protocol proved robust, with no data collection failures during deployment.

Approximately 1000 transmissions were received by each of the six motes over three trials conducted on different days. From 20°C to 60°C the mean decrease in RSS for a receiver was 7.2 dB, with a minimum of 6.5 dB and a maximum of 8.2 dB, and a standard deviation of 0.70. Figure 10 shows a time series view of RSS against temperature measured by a single receiver for a single trial. Figure 1(a) on pg. 4 shows the same data in the temperature domain.

The example plots clearly illustrate the linear relationship of signal strength and temperature. Therefore the *Temperature Loss* ($L_{out}(T)$) outdoors in dB from transmitter and receiver

Table 2. Protocol for wireless signal measurements between a pair of motes outdoors. First the fixed mote sends a message burst to the movable mote, then the movable mote sends a burst to the fixed mote, and finally both motes measure RF noise and environmental parameters.

Fixed Mote State	Movable Mote State	Event or Duration	Description
SYNC_LISTEN	SYNC_LISTEN	Receive time sync beacon (approx. 5 sec)	Listens for Syncmote beacon, then sets sync timer for 40 seconds.
SEND_SETUP	RSS_LISTEN	4 sec	Synchronization/wait time
RSS_SEND	RSS_LISTEN cont'd.	9 sec	Fixed mote sends test message burst, which should take 5 sec, but sometimes takes 7 sec.
RSS_LISTEN	SEND_SETUP	4 sec	Synchronization/wait time
RSS_LISTEN cont'd.	RSS_SEND	9 sec	Movable mote sends test message burst.
READ_SENSORS	READ_SENSORS	4 sec	Collects RSS noise reading (average of 20 samples), temperature, humidity, and sometimes battery voltage. Turns off radio.
SYNC_SLEEP	SYNC_SLEEP	Sync timer timeout (approx. 10 sec)	Sleep buffer to conserve power. Turns on radio just before transition to SYNC_LISTEN state.

combined may be expressed as:

$$L_{out}(T) = 0.179(T - 20), \tag{3.2}$$

where T is the temperature in the range $20°C \leqslant T \leqslant 60°C$. The combined loss is very close to that reported in the CC2400 transceiver's datasheet.

The maximum RSS loss outdoors is within 1 dB of the maximum loss measured by the earlier lab experiments. In both environments the transmitter and receiver were heated, but outdoors the propagation medium was heated as well. These results support our conclusion from the lab experiments that the RSS loss is due to heating the hardware rather than the medium.

For the rest of this study we define temperature loss $L(T)$ as $L_{out}(T)$. We use the outdoor experiment results due to the larger sample of motes tested and larger data set generated by three separate trials for each mote.

3. Path Loss Models

To assess the importance of the variation in signal strength with temperature, next we use well known path loss models to predict the corresponding variation in communication range. The widely used *Log-Distance* path loss model provides a simple way to translate signal strength to communication range. Received power P_r is proportional to a power n of transmission distance d:

$$P_r \propto [d/d_0]^n,$$

or in dB-class units:

$$P_r(dB) = P_0(dB) - 10\, n \log(d/d_0), \tag{3.3}$$

where P_0 is the received power measured at the reference distance d_0 (usually 1 m for low power implementations), and n is the *path loss exponent*, a parameter that depends on the environment where communication occurs, with values typically between 2 and 4 [30].

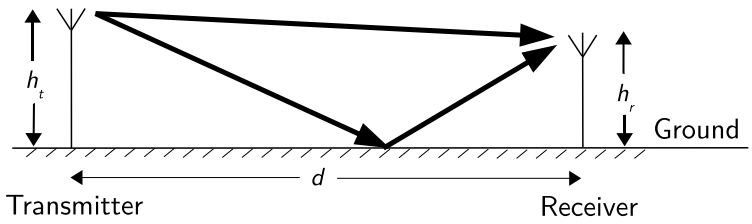

Figure 11. Direct and reflected signal paths that form the basis of the two-ray model.

A second path loss model, the *Two-Ray* model, is well-suited to open outdoor environments, as in the experiment to measure decrease in communication range described in Chapter 4. This model describes the received signal as a combination of a component propagated directly through free space together with a component reflected from the ground, as shown in Figure 11 [29]. The accuracy of the two-ray model in an uncluttered outdoor environment has been verified experimentally, for example in [12].

The two-ray model specifies that at relatively close distances between nodes, receiver power falls off at an overall rate proportional to d^2 although there are wide oscillations due to interference patterns between the direct and ground-reflected waves. However, when the distance is much greater than $\sqrt{h_t h_r}$ (for transmitter and receiver antenna heights h_t, h_r), the received power decreases smoothly at a rate proportional to d^4; specifically:

$$P_r = P_t G_t G_r \frac{{h_t}^2 {h_r}^2}{d^4} \tag{3.4}$$

where P_t is the output power at the transmitter and G_t and G_r are the antenna gain for the transmitter and receiver.

4. Expected Reduction in Range at High Temperatures

For a digitally modulated signal in the absence of interference, radio sensitivity P_s is defined as the maximum power level P_r at which the receiver begins to experience packet loss.[1] Below this

[1]For IEEE 802.15.4, P_s is based on a packet error rate of 1%.

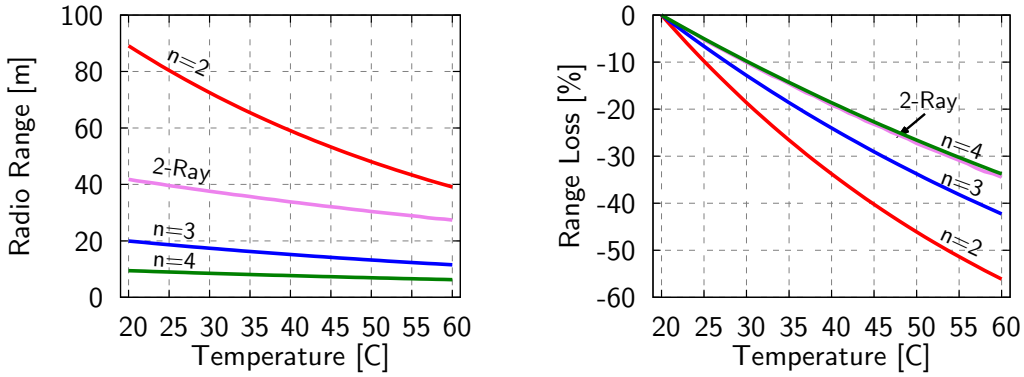

(a) Absolute reduction **(b) Relative reduction**

Figure 12. Maximum communication range R_{max} against temperature for log-distance and two-ray models. Simulation parameters: $P_t = -10$ dBm, $P_0 = -55$ dBm, $d_0 = 1$ m, $P_s = -94$ dBm, and $h_t = h_r = 0.5m$.

power level, packet loss increases rapidly. Given the decrease in signal strength with distance shown in the path loss models above, we define the communication range limit R_{max} as the maximum value d such that $P_r(d) \geqslant P_s$. Our signal strength experiments have shown that temperature further attenuates the received signal, and thus we expect it to reduce the radio range. Therefore we add the term for temperature loss defined in (3.2) to the basis for R_{max}:

$$P_r(d) - L(T) \geqslant P_s. \tag{3.5}$$

So given a pair of wireless devices and fixed parameters for the path loss model, the value of R_{max} becomes a function of the temperature. Figure 12 graphs $R_{\text{max}}(T)$ for round values of the log-distance model's path loss exponent n and for the two-ray model, in absolute and relative units. For convenience the simulation parameters used for these plots are the actual parameters of the validation experiments in the next chapter. In all cases the range decreases significantly over 40°C, with reductions of 34% (log-distance, n = 4), 56% (log-distance, n = 2), and 34% (two-ray) of the original value.

CHAPTER 4

Measured Impact on Data Collection and Communication Range

For a network designer the importance of the 1.8 dB/10°C decrease in RSS is its impact on link quality and sensor network applications. This chapter uses the expected reduction in communication link range from the last chapter to simulate the performance of a typical data collection network. Then we describe the outcome of an outdoor experiment to confirm the predicted decrease in range.

1. Simulated Impact on a Data Collection Deployment

Outdoor applications such as environmental sensing and precision agriculture monitor slowly varying signals such as temperature and soil conditions over large areas. To keep deployment and maintenance costs low, sensor nodes often are placed in a sparse configuration to minimize the number of units required to cover the monitored area. However, since messages must be routed through a few radio links, communication intrinsically is more prone to failures, and accurate pre-deployment analysis of the link budget is critical to ensure reliable networking.

In this section we use simulation to show the effect of temperature on network connectivity and performance for a *source-to-sink* data collection application. As with any simulation, certain assumptions are made to simplify its operation. For example we assume radio links are symmetric and all motes share an identical minimum RSS level that achieves 1.0 PRR. However, given these simplifications, the simulation demonstrates that a network configuration with good performance at low temperatures may deteriorate significantly at high temperatures as a result of the loss in signal strength. Figure 13 conceptually illustrates the phenomenon of reduced connectivity in a network as temperatures increase, with the dashed line representing the path of a message as it is forwarded toward a sink node. At low temperatures (blue disks) the range of reliable communication for each link overlaps; however, at high temperatures (magenta disks) the message path includes less reliable links.

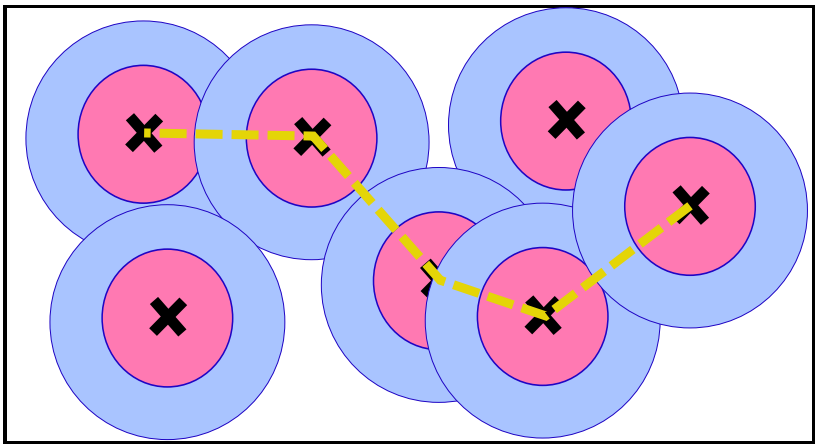

Figure 13. Overhead view of a message path through a network of transceivers, where the blue disks represent reliable communication range at low temperature and the magenta disks represent reduced range at high temperature.

Consider a relaxed grid topology outdoors, where 49 nodes are deployed over a square region measuring approximately 140 m on each side, with a collection sink at one corner as shown in Figure 1(b,c) on pg. 4. In general a grid topology is suited to measurement of the distribution of a physical characteristic over a given area. In this simulation actual node positions vary from the true grid points by a normally distributed amount, with a standard deviation of 20% in both the x and y directions. This variability is intended to simulate node placement based on a grid but extended to also sample other parameters such as directional slope or exposure (north, southwest, etc.), points of high or low elevation, type of vegetation, or type of soil.

We model an area composed of a grassy field with some underbrush, which provides a path loss exponent of 3.6 for the log-distance model, based on actual measurements of such an area [30]. In the simulation we measure node connectivity over the temperature range from 20°C to 60°C. Using (3.5), the mean internode distance of 23.3 m in the x and y directions corresponds to the extent of the reliable communication range at 52°C, near the maximum temperature. Relative to one of the disks in Figure 13, this distance is in the blue region of reliable connectivity at low temperature, but near the perimeter of the magenta disk of reliable connectivity at high temperature.

We obtain network connectivity using the *log-normal shadowing* model [29], which extends the log-distance model to account for additional real-world variability in received power due to obstructions in the deployment area. The received power (in dBm) at distance d is modeled as a random variable:

$$P_{rs}(d) = P_r(d) + X_\sigma, \tag{4.1}$$

where $P_r(d)$ is the value defined in (3.3) for the log-distance model, and X_σ is a zero-mean random variable with normal distribution $\mathcal{N}(0, \sigma_{\text{dB}})$. The shadowing variance parameter of 8.4 dB is based on the same grassy field measurements as the path loss exponent [30].

For each trial the RSS for each possible node pair was determined by sampling from (4.1), with the link quality assumed to be symmetric. If the RSS was above a threshhold value of -94 dBm, the CC2420 radio's sensitivity level, the two nodes were assumed to connect with 1.0 PRR. If the RSS was between -94 dBm and -96 dBm, the two nodes were assumed to connect with a PRR that decreased linearly over that range to a minimum of 0.4. This band of connectivity is known as the transitional region of communication quality [45]. The cost of transmission is expressed as estimated transmission count (ETX) [6]:

$$ETX = \frac{1}{PRR_f \times PRR_r}, \tag{4.2}$$

where PRR_f and PRR_r are the packet reception rate in the forward and reverse directions for a given pair of motes. As mentioned above, we simplify this calculation to use the same PRR value in both directions. ETX accounts for both the original data transmission and the receiver's acknowledgement. At high PRR, ETX is near 1, and at 0.4 PRR, ETX is around 6.

Then to simulate the effect of temperature, RSS from all transmitters was uniformly reduced by the linear loss due to temperature in (3.2), derived from our signal strength experiments. The effect on connectivity was measured from 20°C to 60°C at 5°C intervals.

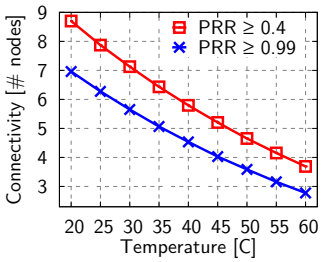

(a) Mean node connectivity

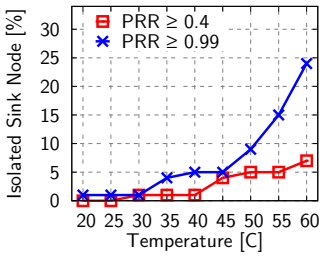

(b) Networks where the sink node is reachable by at most 10% of all network nodes.

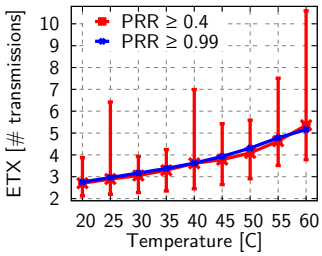

(c) Mean ETX for data collection over all source nodes to the sink; bars show range of mean including marginal links. Excludes networks in (b) with isolated sink.

Figure 14. Connectivity and performance for a 7x7 node simulation of multi-hop data collection over 40°C range. Node positions generated using a relaxed grid deployment model. Wireless parameters: $P_0 = -39$ dBm, $d_0 = 1\,m$, $n_p = 3.6$, $\sigma_{\mathbf{dB}} = 8.4$ dBm. Plots show two link quality levels: $Ps = -94$ dBm for reliable 99% PRR, and -96 dBm for marginal 40% PRR.

100 trials were performed to generate the results shown in Figure 14, which show two measures of link quality and performance: use of only high quality links near 1.0 PRR, and inclusion of marginal links down to 0.4 PRR. The simulations begin with robust node connectivity at 20°C that decreased at a rate of approximately one link per 10°C. Although not included in the figure, overall network connectivity remained high, even at high temperatures. The median network connectivity at 60°C was 92% of nodes for high quality links and 98% for marginal links. However as shown in Figure 14(b), in some cases the sink node became isolated from the rest of the network. Specifically we define an *Isolated Sink* network as one where the sink node is reachable by less than 10% of the nodes. At 60°C approximately one-quarter of networks had lost reliable connectivity with the sink. Figure 1(c) on pg. 4 shows two examples of lost connectivity: the link to node 1, the sink node, is of low quality, and node 7 is unreachable (PRR less than 0.4).

The simulation then used PRR to measure ETX to the sink for each node. The doubling of average ETX over the 40°C range as shown in Figure 14(c) indicates that a network can expect increased energy usage and latency in message delivery. The graph excludes networks with an

Figure 15. Experimental setup on a leveled agricultural field with each mote elevated to 0.5m and wrapped in a plastic bag. Each mote in the Fixed group exchanged packets with each mote in the Movable group.

isolated sink node since ETX is undefined. Across the range of temperatures, ETX values when considering only high quality links are virtually identical to ETX values when including marginal links. However, this performance value for high quality links excludes a larger number of isolated sink networks than are excluded when also considering marginal links.

2. Experimental Validation of Range

Maximum communication range affects critical parameters in outdoor sensor network deployment like mote density and placement, antenna strength, and signal power levels. Therefore we performed an experiment to measure the effect of temperature on range to validate the expected values from the path loss models presented in the previous chapter against actual measurements of R_{max} over a 40°C range of temperatures.

Wireless communication is subject to reflection from large flat surfaces, diffraction around edges such as the corner of a building, and scattering from smaller objects. To minimize these effects in an outdoor environment, the experiment was sited in an open agricultural field that had been plowed and leveled, as shown in the photograph in Figure 15.

Six Telos-class motes were separated into two groups of three, a *fixed* group whose position remained the same across succeeding runs, and a *movable* group whose position was altered with

each run.[1] We tested the eight distances from 26 m to 40 m at two meter intervals. Each mote was oriented vertically facing the opposite group, with the internal antenna at the top and the battery pack behind. The motes were supported so that the antenna was 0.5 m above ground,[2] and each was covered with a white plastic bag that resulted in solar-heated maximum temperatures around 60°C.

Each mote served as both transmitter to the three motes in the opposite group, and as a receiver for each of those other three motes. Each transmission session between a pair of motes included 100 identical packets with a payload size of 25 bytes, with one packet sent every 50 ms. A cycle of testing each unique transmitter-to-receiver pair required nine minutes, and a complete trial at a given distance lasted approximately 24 hours. For each 100-packet session we collected PRR and mean RSS for signal and noise as well as the RSS standard deviation. The data was collected over several weeks in late summer with typical weather for this time period: high temperatures around 40°C, lows in the low-20s°C, and moderate humidity.

Implementation of this sampling system required significant coordination to maintain synchronization among the six motes. We used the same procedure as described for the signal strength experiments in Chapter 3.

3. Experimental Results

As mentioned in the previous section, our primary goal was to measure $R_{\max}(T)$, the limit for reliable communication, where a receiver just begins to lose packets from the transmitter. These results use transmissions with a PRR of 0.95 to 0.98 as the reliable communication limit.[3] The

[1] We considered two basic designs for the experiment: 1) vary link distance quickly to find the reliable communication limit at a given temperature during the day, or 2) hold mote distance constant and allow the daily cycle of heating and cooling to alter the temperature. Neither method is perfect, but we chose the second method as simpler to execute and easier to test several motes simultaneously. Within this second method we also chose to test several motes at the same distance with each experimental run rather than arraying the motes over a range of distances with each run. Our choice allows for more direct comparisons of mote performance.

[2] The height was chosen to provide a realistic distance between the mote groups yet also to ensure completely reliable communication, even under the worst conditions, with other external motes that controlled and coordinated the experiment.

[3] We omitted transmissions with PRR of 0.99 because they raised the standard deviation of temperature readings from 1.9°C to 3.0°C due to occasional spurious loss of a packet at low temperatures.

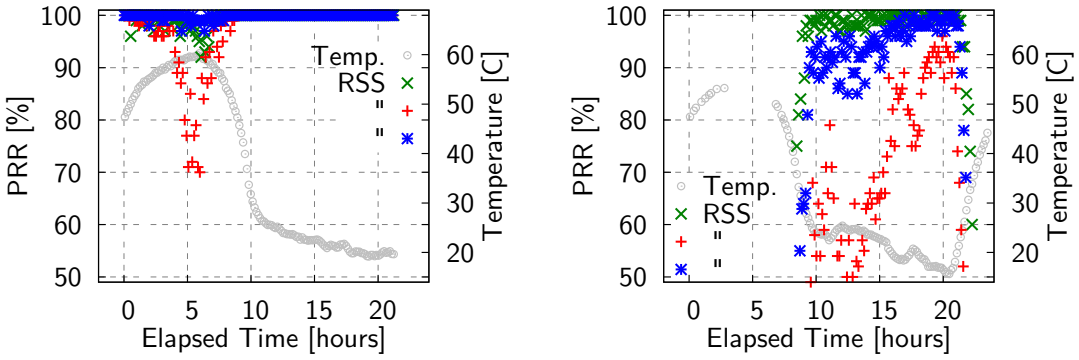

(a) 30 meters; reliable to 58°C.

(b) 40 meters; reliable only to 20°C. Missing temp. from 4-6 hrs due to 0 PRR.

Figure 16. Example results for transmitter mote F3 with three receiver motes at near and far distances.

temperature reported for a given distance is the mean for all packets received within the target PRR values.

Figure 16 shows raw results over time for transmitter F3 at near and far distance extremes for reliable communication. At 30 m the motes fall below reliability briefly at an average of 58°C. In contrast at 40 m the motes attain reliability for a relatively short period when temperatures fall to an average of 20°C. These graphs also show one of the receiver motes (in red) with worse performance. For example it barely reaches reliable communication at 40 m while the other two receivers are reliable at higher temperatures for longer time periods. The poor performer is mote M2, which also was a poor transmitter as described below.

Table 3 and Figure 17 show the loss in communication range as a function of temperature from 20°C to 60°C for each transmitter, with a mean loss in communication range of 26% overall. The range values are calculated from a linear interpolation of the actual measurements of maximum temperature at fixed distances.[4]

The loss in communication range of 10.4 m is 28% less than the 14.4 m predicted by the

[4]The linear fit is slightly better than a quadratic fit.

Table 3. Loss and variability in maximum communication range based on linear fit. Two of the rows that report mean values exclude one or more motes, which are designated by an "x" before the mote ID.

Transmitter Mote ID	20°C Fit Distance (m)	60°C Fit Distance (m)	Loss (m)	Loss (%)	Std Dev from Mote Fit (m)	Std Dev from Mean Fit (m)
F1	39.5	28.8	10.8	27.3	1.4	2.0
F2	38.3	30.0	8.3	21.8	2.5	3.3
F3	39.1	28.8	10.3	26.1	1.4	2.7
M1	43.3	31.2	12.0	27.7	1.6	3.4
M2	36.5	26.0	10.6	28.8	1.6	4.4
M3	42.0	31.4	10.6	25.1	1.6	3.1
Mean	**39.8**	**29.4**	**10.4**	**26.1**	1.7	3.1
Mean xF2	39.6	29.1	10.5	26.4	1.5	3.1
Mean xF2 xM2	41.1	30.4	10.7	26.0	1.4	1.9
Two-Ray	41.8	27.4	14.4	34.5		
n = 2.3	49.6	25.5	24.1	48.6		

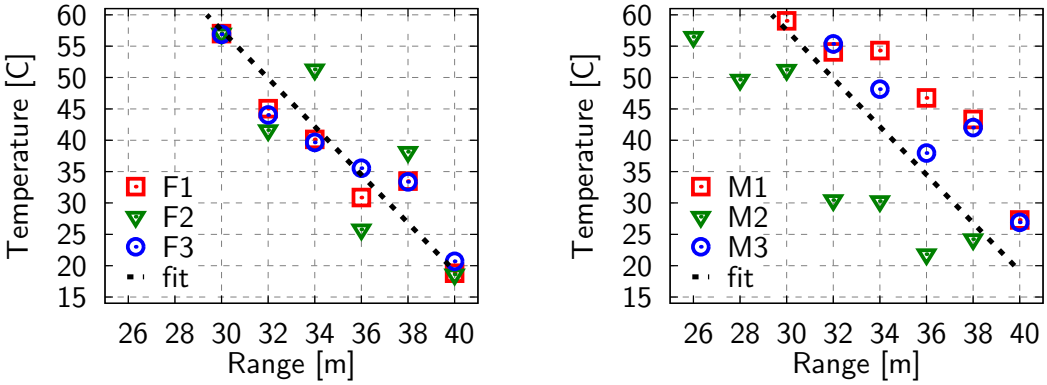

(a) Fixed transmitters **(b) Movable transmitters**

Figure 17. Maximum temperature for reliable communication for each transmitter at distances from 26 m to 40 m. Each graph includes the mean linear fit over all transmitters, which provides a common reference between the two groups.

two-ray model. However, the two-ray model prediction is much closer than the best fit log-distance model exponent of 2.3. This greater accuracy of the two-ray prediction is expected since the experimental location was chosen to match the environment used by that model, while the log-distance model is more generic.

The performance of two transmitters varied noticeably from their peers. Mote M2 clearly showed a shorter maximum range: at 60°C it was 2.8 m less than the any of its peers. Also its standard deviation from the mean fit was 1 m greater than any other transmitter. Mote F2 showed significantly greater variability in the actual distance for a given temperature relative to its linear fit, with a standard deviation almost 1 m greater the next most variable mote.

Given the exceptional variations from F2 and M2, the results table also includes two rows with mean statistics that exclude readings where these motes were transmitter or receiver. The row "Mean xF2" excludes only F2, and "Mean xF2 xM2" excludes both motes. Neither case significantly altered the overall mean decrease in range.

CHAPTER 5

Model and Interpretation of Thermal Effects on the Transceiver

In Chapter 3 we concluded that the radio hardware rather than the propagation medium caused the loss in signal strength with temperature. This chapter first describes the components of a transceiver and models signal flow through them. Then we use the model to interpret the results from some of our experiments to understand the mechanisms behind the temperature-based loss.

1. Transceiver Components, Signal Path, and RSS Measurement

The high level components of the CC2420 low-power transceiver are shown in Figure 18, derived from the datasheet. A message is transmitted by the following sequence: the transmitter modulates digital data into a sequence of bits based on an agreed protocol, converts the bit sequence into an analog *radio frequency* (RF) signal, and then amplifies the signal to a power level strong enough to propagate some useful distance. For example the widely used IEEE 802.15.4 communication protocol uses *Direct Sequence Spread Spectrum* (DSSS) to modulate the data signal into a bit stream and encodes each bit in the analog signal with a form of *Phase Shift Keying* (PSK) [16]. The figure shows a *Digital to Analog Converter* (DAC), a signal mixer used to generate the precise 2.45 GHz signal, a *Power Amplifier* (PA) that boosts signal strength to approximately 0 dBm or 1 mW at full power, and finally an antenna to efficiently radiate the signal into the air.

After traveling some distance, the receiver amplifies the much weakened signal, reverses the encoding from analog back to a bit sequence, and demodulates the sequence into the original data. The incoming signal may be as weak as -95 dBm or 0.3 pW, so a *Low Noise Amplifier* (LNA) is employed to magnify the signal to a usable level while minimizing the introduction of noise. The frequency mixer reduces the signal to the low MHz range, where additional amplification and filtering occur. The figure finally shows an *Analog to Digital Converter* (ADC) and demodulation steps.

RSS measurement also occurs at the end of the reception sequence; however the RSS value

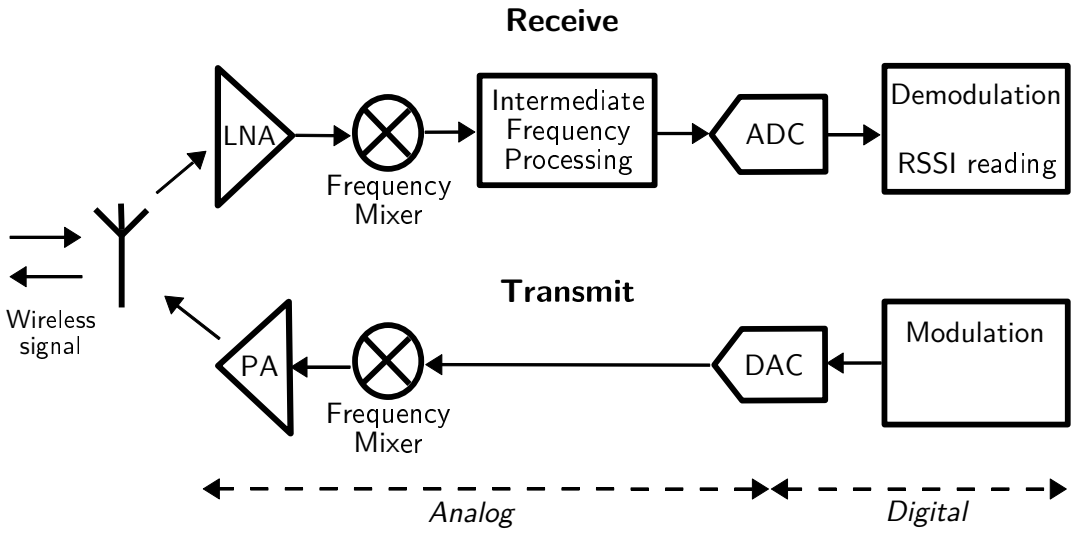

Figure 18. Components and signal path for transmission and reception

nominally reports signal power received at the *beginning* of the sequence, from the antenna. Therefore the reported RSS must account for the signal gain and noise added by the receiver. The position of the RSS measurement explains the decrease in signal strength measured in the lab when only the receiver was heated, as shown in Figure 7(b) on pg. 13. The signal strength input to the receiver did not change as the receiver was heated; instead temperature affected the receiver's signal processing as measured at the end of the process.

Finally, transmission is a relatively simple operation compared to reception because its primary requirement is to amplify a signal of its own generation. Reception is more complex because it must amplify the desired signal, filter out undesired signals also present in the wireless channel, and minimize imposition of its own noise on the weak incoming signal.

2. Modeling Signal, Noise, and Power Gain

The model for the signal channel through the transceiver is based on *Additive White Gaussian Noise* (AWGN). Within the channel, signal $s(t)$ and noise $n(t)$ over time are combined such that the measured signal $m(t) = s(t) + n(t)$. The transmitter or receiver then may be modeled as a

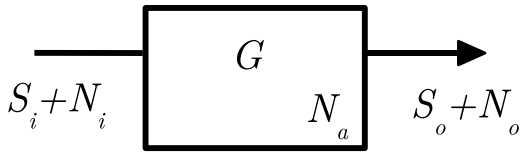

Figure 19. Model of signal S and noise N through the analog portion of a transceiver, including gain G and noise N_a added within the transceiver.

two port black-box as shown in Figure 19. One port accepts signal and noise into the channel, and the second port outputs a linear transformation of the input:

$$\begin{aligned} S_o + N_o &= G(S_i + N_i) + N_a, \\ S_o &= GS_i, \\ N_o &= GN_i + N_a \end{aligned} \tag{5.1}$$

where G is the gain factor implemented by the amplifiers described for Figure 18, especially the LNA and PA. In addition the transceiver components inevitably add some noise N_a of their own.

In practice we are not concerned with noise generation at the transmitter. As the CC2420 datasheet shows, the power level of spurious transmissions average approximately -50 dBm when the desired signal is at 0 dBm. So at any realistic reception distance, the spurious signals will be at a power level lower than the noise floor of the receiver. Therefore we ignore the noise contributions, and the output signal is simply $S_o = GS_i$.

In contrast to the transmitter, the receiver must account for noise because the incoming signal power level may be near the noise power level. A relevant figure of merit for a receiver is its *Noise Factor* (F), defined as the degradation of *signal-to-noise ratio* (SNR) from input to output [1], and related to (5.1) above:

$$F = \frac{S_i/N_i}{S_o/N_o} = \frac{GN_i + N_a}{GN_i} \tag{5.2}$$

When noise factor is expressed in dB units, it is referred to as *noise figure* (NF). For the CC2400

receiver, the noise figure is approximately 10 dB [35].

3. Physical Basis for Thermal Effects

Transceiver properties that change with temperature, like gain, imply physical mechanisms to actually generate the measured changes. Transistors fundamentally provide the gain in an amplifier like the LNA, and the dominant thermal effect on *complementary metal-oxide-semiconductor* (CMOS) transistor performance is the reduction in electron/hole mobility as temperature increases [43]:

$$\mu(T) = \mu_0 \left(\frac{T}{T_0} \right)^m , \tag{5.3}$$

where μ is the mobility, T_0 is 300$\dot{\text{K}}$ and m is between -1 and -2 [2].

Wu *et al.* [43] describes a cascode-style LNA for which this inverse relationship of mobility with temperature has the effect of reducing the transconductance gain[1] with temperature and increasing the noise figure. The experimental scenarios described below show that changes in gain and noise figure with temperature are two likely sources of the change in experimental signal strength measurements.

4. Heated Transmitter

In the next few sections we use the model presented earlier in this chapter to interpret experimental observations of signal strength loss as temperature increases. The depth of this analysis is qualitative: the goal is to assign the loss to a mechanism, like decreased gain or increased noise, and then identify the components likely to participate in the mechanism. A quantitative analysis would require more detailed measurements at the component level.

In this analysis we express a model component like gain as a function of temperature at two input values: near room temperature *(lo)* and at some elevated temperature *(hi)*. Then a multiplicative factor equates the readings at the two temperature levels, for example: $G(hi) = G(lo)\Delta_G$. We

[1] A model of transistor performance that measures current output per voltage input.

use a multiplicative factor rather than an additive one for ease of manipulation and for correspondence to power measurements in watts.

The first scenario is based on the laboratory experiment described in Chapter 3 that heated the transmitter while the receiver remained at room temperature. In terms of the two port model in (5.2), the transmitter was programmed to output a given signal level S_o, but it does not measure this quantity directly. Instead the transmitter assumes the input signal S_i is fixed, and then the sets the power amplifier gain G to generate the required signal level. So the difference in output from high temperature to low temperature is:

$$\begin{aligned} \frac{S_o(hi)}{S_o(lo)} &= \frac{S_i(hi)G(hi)}{S_i(lo)G(lo)} \\ &= \Delta_G \Delta_{Si} \end{aligned} \tag{5.4}$$

We found the transmitter power decreased by 5 dB from 25°C to 65°C. We therefore attribute this decrease to a combination of loss of gain from the power amplifier and signal loss from the DAC or the mixer.

5. Heated Receiver Noise

During the outdoor signal strength experiment described in Chapter 3, noise power N_o also was measured by sampling RSS when no signal was incoming. Using (5.2) and the definition of incoming thermal noise:

$$N_o = FN_i = FkT_0B \tag{5.5}$$

where F is noise factor, k is Boltzmann's constant, T_0 is the source temperature in Kelvin, and B is the equivalent noise bandwidth, assumed to be the 802.15.4 channel bandwidth of 3 MHz [26]. Solving for N_o with the CC2400 noise figure of 10 dB yields approximately -99 dB, which is near our mean experimental RSS measurement for N_o of -96 dB at 20°C.

As shown in Figure 20(a) for a single mote outdoors, noise power decreased with tempera-

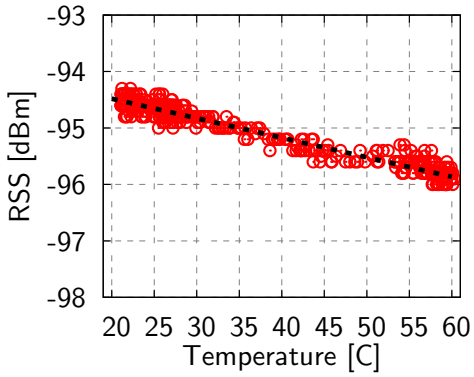

(a) Noise power outdoors, collected over a 24-hour period.

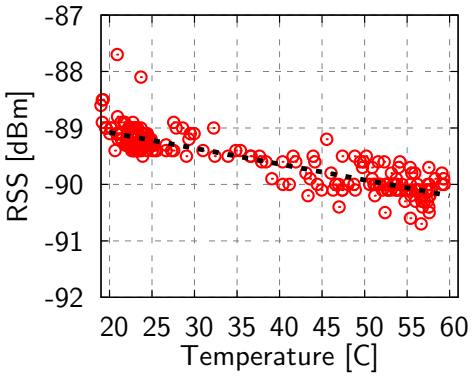

(b) RSS outdoors for packets received at the reliable communication threshhold. Includes data from several transmitter/receiver distances to capture the full temperature range.

Figure 20. RSS measurements for noise alone and for packets at constant PRR/SNR for a single mote.

ture. For all six motes outdoors the mean loss in noise power from 20°C to 60°C was 1.3 dB, with a standard deviation of 0.4. This result is counter-intuitive because (5.5) specifies that noise power *increases* slightly with temperature.

We use the model to interpret how output noise changes with temperature:

$$\begin{aligned} \frac{N_o(hi)}{N_o(lo)} &= \frac{G(hi)N_i(hi) + N_a(hi)}{G(lo)N_i(lo) + N_a(lo)} \\ &= \Delta_G \Delta_F \Delta_{Ni} \end{aligned} \tag{5.6}$$

As described in Section 3 of this chapter, we expect gain Δ_G to decrease with temperature and noise figure Δ_F to increase. We expect incoming noise Δ_{Ni} to increase approximately 0.2 dB outdoors. Therefore the measurements indicate the decrease in amplifier gain outweighs any increase in the other two terms.

6. Heated Receiver with Constant PRR/SNR

The transmission range experiment described in Chapter 4 measured the decrease in the maximum distance for reliable communication as temperature increased. Packet loss begins (and

PRR begins to decrease from 1.0) when the probability of a bit error P_e in the received signal begins to increase from near zero. For IEEE 802.15.4 *Offset Quadrature Phase Shift Keying* (OQPSK) modulation, P_e is $Q(\sqrt{2E_b/N_0})$, where Q is the Gaussian Q-function, E_b is the energy per bit, and N_0 is the noise power spectral density. Relevant to this discussion, E_b/N_0 also is related to the *Signal to Noise Ratio* (SNR) by:

$$\text{SNR} = \frac{E_b R}{N_0 B} \tag{5.7}$$

where R is the data rate and B is the channel bandwidth.

Since P_e and SNR both are functions of E_b/N_0, we expect that if PRR is constant, then SNR will remain constant too. However as transmission distance increased in the experiment, the temperature to reach this threshold PRR decreased. Therefore we can compare the measured RSS at the threshold PRR at different temperatures, just as we compared the RSS for noise power at different temperatures in Section 5.

Since we found noise power decreased with temperature, (5.7) indicates we also expect the measured signal power to decrease with temperature to maintain a constant SNR and PRR. Indeed the outdoor transmission range experiment measured a decrease in RSS, as shown for one mote in Figure 20(b). Overall the mean loss in RSS from 20°C to 60°C was 0.94 dB, with a standard deviation of 0.4.

Constant PRR and SNR in this experiment provide more information to interpret the result against the transceiver model. The meaning of SNR provides an expression for $S_i(lo)$:

$$\begin{aligned} \frac{S_o(lo)}{N_o(lo)} &= \frac{S_o(hi)}{N_o(hi)} \\ \frac{S_i(lo)G(lo)}{G(lo)N_i(lo)) + N_a(lo)} &= \frac{S_i(hi)G(hi)}{G(hi)N_i(hi)) + N_a(hi)} \\ S_i(lo) &= \frac{S_i(hi)N_i(lo)}{\Delta_F N_i(hi)} \end{aligned} \tag{5.8}$$

Then we use this value to analyze the ratio of RSS at high and low temperatures:

$$\begin{aligned}\frac{S_o(hi)+N_o(hi)}{S_o(lo)+N_o(lo)} &= \frac{G(hi)[S_i(hi)+N_i(hi)]+N_a(hi)}{G(lo)(S_i(lo)+N_i(lo))+N_a(lo)} \\ &= \frac{\Delta_G(S_i(hi)+F(hi)N_i(hi))}{\frac{S_i(hi)N_i(lo)}{\Delta_F N_i(hi)}+F(lo)N_i(lo)} \\ &= \Delta_G\Delta_F\Delta_{Ni} \end{aligned} \tag{5.9}$$

Remarkably, the expression for this ratio is the same as when comparing only noise values, as shown in (5.6). In terms of the signal model, an increase in noise figure (positive Δ_F) would require an increase in RSS to maintain constant SNR. Since RSS decreased, reduction of gain is the likely source, as we found in Section 5 for the noise values.

Overall, the analysis of the experimental results with the signal model has shown that as temperature increases, a decrease in gain, combined with reduced input signal level from the transmitter, accounts for the reduced signal strength readings. For the receiver, gain affects the RSS measurement because RSS is sampled *after* amplification. Our analysis indicates the thermal properties of the transmitter's power amplifier and the receiver's low-noise amplifier are the main source of the reduction in output power and sensitivity as temperature increases.

CHAPTER 6

Summary, Recommendations and Future Work

This thesis was inspired by observation of a daily variation in RSS for low-power wireless sensor nodes placed outdoors in the summer. Initial experiments in a thermal chamber reproduced the effect and localized the source to the mote hardware rather than the propagation medium; both transmitter and receiver contributed to the loss. Further experiments outdoors measured a linear 7.2 dB decrease in signal strength over the 40°C range from 20°C to 60°C. Chapter 3 presented an equation to express this reduction as a function of temperature.

Next the implications of the loss in signal strength for transmission range and outdoor data collection were presented. The log-distance model expected a range loss of 34% to 56% as the path loss exponent decreased from four to two; the two-ray model also expected a 34% loss. In Chapter 4 a simulation of a source-to-sink data collection network based on the log-normal extension to the log-distance path loss model found that a network with good connectivity and throughput at lower temperatures may deteriorate significantly over the 40°C range. Specifically, the simulation found node connectivity was reduced by half and ETX doubled, which increases node energy usage and transmission latency. Communication range loss with temperature was measured in a leveled agricultural field. Range decreased by 26% from 20°C to 60°C, near but somewhat less than the 34% value predicted by the two-ray model.

Finally, Chapter 5 analyzed the components of a low-power transceiver to understand the mechanism behind the signal strength loss. In general the performance of transistors was found to decrease with temperature; therefore the transmitter's power amplifier and the receiver's low-noise amplifier were likely sources of the decrease in signal gain. A two-port linear model of a transceiver incorporating signal, noise, and gain was described. A temperature-based decrease in RSS was found in our transmission range experiments that was consistent with a loss of transceiver gain from the model.

1. Recommendations

Our results direct the designer of a low-power network in an environment with large temperature variations to account for reduced signal strength and connectivity. In general the strategies to improve performance include reduction in temperature variation or compensation for the decrease in signal strength. Below are several recommendations:

- Read the manufacturer data sheet for the mote and transceiver used in the deployment for specification of a temperature-based RSS variation.
- In an environment with significant temperature variation, include the term for signal strength loss with temperature, $L_{out}(T)$, derived in (3.2), in overall link budget calculations. In particular when using the log-distance model for range estimation, beware of an environment with a low path loss exponent, such as a base station elevated above a sensor node field. Such an environment may experience range loss near 50% over a 40°C temperature range.
- Evaluate sensor placement, enclosure materials, and thermal insulation and venting to understand and mitigate temperature variation due to exposure to the sun or other heating sources.
- Increase received signal power by using antennas with higher or more directional gain, or reduce path loss by avoiding obstructions or increasing antenna height.
- Reduce link distance between sensing motes or add intermediate relay nodes.
- If the application tolerates communication delay, defer communication to cooler time periods to increase reliability.

2. Future Work

The research presented in this work suggests further experiments to expand its scope or to gain a deeper understanding of a particular effect. We conclude with the following topics for continued investigation.

Measure thermal effects on other low-power wireless motes: Our experiments used only the

CC2420 transceiver in Telos-class motes; however, the datasheets for the Atmel RF230 transceiver [4] used in the Crossbow IRIS mote and the Digi XBee module [8] also omit a discussion of the impact of temperature on transmission and reception.

Implement software-based thermal compensation of RSS levels: Lin, *et al.* [21] provides an example of generic RSS compensation; however, an on-board temperature sensor may be used to trigger compensation before the effects on RSS become noticeable. Also, the transceiver may provide fine-grained control over amplifier power levels beyond the basic output power level, for example by tuning *automatic gain control* (AGC).

Expand the mote simulation to evaluate the influence of input parameters: For the log-normal model, vary the path loss exponent and random shadowing variable. Alter the distance between grid points and the amount of variation between actual node positions and true grid points. Try other path loss models, like the two-ray model. Try a different layout topology; rather than a grid, use a clustered arrangement or random placement.

Experimentally verify our simulation of the impact of temperature variation on a data collection application: Quantify the increased energy usage and transmission latency as temperature increases. Investigate the value of shorter link distance for nodes near the sink node to reduce the possibility of its isolation from the rest of the network.

The results for the outdoor range experiment found a mean loss in communication range of 10.4 m, 28% less than the 14.4 m predicted by the two-ray model. Investigate the source of this discrepancy: For example validate the accuracy of the two-ray model in this environment at a constant temperature. Also the short antenna height of 0.5 m may have magnified the effect of small variations in the level of the ground, so compare the results at a height of 1 m. In addition each mote was powered by two AA batteries. As battery power was depleted over a day-long trial, voltage decreased, which may influence mote output power and receiver sensitivity. Therefore experiment

with a strong, constant power source.

Validate our analysis that reduced gain by the transmitter's PA and the receiver's LNA are significant sources of the loss in signal strength: Circuit measurement tools may provide insight for black box properties of a commercial transceiver, or circuit design tools may permit an amplifier simulation.

REFERENCES

[1] AGILENT. 2006. Application Note 57-1. *Fundamentals of RF and Microwave Noise Figure Measurements*.

[2] ARORA, N. 2006. *MOSFET Modeling for VLSI Simulation: Theory and Practice*. World Scientific.

[3] ASADA, G., DONG, M., LIN, T., NEWBERG, F., POTTIE, G., KAISER, W., AND MARCY, H. 1998. Wireless integrated network sensors: Low power systems on a chip. In *Solid-State Circuits Conference, 1998. ESSCIRC'98. Proceedings of the 24th European*. 9–16.

[4] ATMEL. 2007. AT86RF230 Datasheet. `http://www.atmel.com/dyn/resources/prod_documents/doc5131.pdf`.

[5] BULT, K., BURSTEIN, A., CHANG, D., DONG, M., FIELDING, M., KRUGLICK, E., HO, J., LIN, F., LIN, T.H., KAISER, W.J., MARCY, H., MUKAI, H., NELSON, P., NEWBURG, F.L., PISTER, K.S.J., POTTIE, G., SANCHEZ, H., SOHRABI, K., STAFSUDD, O.M., TAN, K.B., YUNG, G., XUE, S., YAO, J. 1996. Low power systems for wireless microsensors. In *Low Power Electronics and Design, 1996., International Symposium on*. 17–21.

[6] DE COUTO, D. AND BICKET, J. 2003. A high-throughput path metric for multi-hop wireless routing. In *Proceedings of the 9th annual international conference on Mobile computing and networking*. ACM New York, NY, USA, 134–146.

[7] DECAGON DEVICES. 2007. *ECH20-TE/EC-TM Operator's Manual*. Pullman, WA.

[8] DIGI. 2008. XBee/XBee-PRO OEM RF Modules. `http://ftp1.digi.com/support/documentation/90000982_A.pdf`.

[9] DUTTA, P., HUI, J., JEONG, J., KIM, S., SHARP, C., TANEJA, J., TOLLE, G., WHITEHOUSE, K., AND CULLER, D. 2006. Trio: enabling sustainable and scalable outdoor wireless sensor network deployments. In *Proceedings of the fifth international conference on Information processing in sensor networks*. ACM New York, NY, USA, 407–415.

[10] ENERGIZER BATTERY MFG. 2007. Alkaline Manganes Dioxide Handbook and Application Manual. `http://data.energizer.com/PDFs/alkaline_appman.pdf`.

[11] ESTRIN, D. 2007. Reflections on Wireless Sensing Systems: From Ecosystems to Human Systems. In *Radio and Wireless Symposium, 2007 IEEE*. 1–4.

[12] GIORGETTI, G., CIDRONALI, A., GUPTA, S., AND MANES, G. 2007. Exploiting low-cost directional antennas in 2.4 GHz IEEE 802.15.4 wireless sensor networks. In *Wireless Technologies, 2007 European Conference on*. 217–220.

[13] HART, J. AND MARTINEZ, K. 2006. Environmental Sensor Networks: A revolution in the earth system science? *Earth Science Reviews 78*, 3-4, 177–191.

[14] HOLLER, M. 2008. High Density Wireless Soil Moisture Monitoring for Deficit Irrigation Management. http://www.xbow.com/eko/Images/HighDensity,MultipleDepth,WirelessSoilMoisture.pdf.

[15] HOROWITZ, P. AND HILL, W. 1989. *The Art of Electronics*. Cambridge University Press.

[16] IEEE. 2003. IEEE Std 802.15.4-2003. http://standards.ieee.org/getieee802/download/802.15.4-2003.pdf.

[17] IMPACT LAB. 2008. ECH20-TE soil probe driver. http://docs.tinyos.net/index.php/TinyOS_2.x_index_of_contributed_code%23ECH2O-TE_soil_probe.

[18] IMPACT LAB. 2009. Soil Sensor Network at the Desert Botanical Garden. http://impact.asu.edu/soil.

[19] KANG, W., STANKOVIC, J., AND SON, S. 2008. On using weather information for efficient remote data collection in WSN. In *Proceedings of the Fifth Workshop on Embedded Networked Sensors (HotEmNets)*.

[20] KIM, S., DENG, G., GUPTA, S., AND MURPHY-HOYE, M. 2008. Enhancing cargo container security during transportation: A mesh networking based approach. In *IEEE International Conference on Technologies for Homeland Security (HST)*. Waltham, MA, USA.

[21] LIN, S., ZHANG, J., ZHOU, G., GU, L., STANKOVIC, J., AND HE, T. 2006. ATPC: adaptive transmission power control for wireless sensor networks. *The 4th international conference on Embedded networked sensor systems (SenSys)*, 223–236.

[22] MAINWARING, A., CULLER, D., POLASTRE, J., SZEWCZYK, R., AND ANDERSON, J. 2002. Wireless sensor networks for habitat monitoring. In *Proceedings of the 1st ACM international workshop on Wireless sensor networks and applications*. ACM New York, NY, USA, 88–97.

[23] MARTINEZ, K., PADHY, P., ELSAIFY, A., ZOU, G., RIDDOCH, A., HART, J., AND ONG, H. 2006. Deploying a Sensor Network in an Extreme Environment. *IEEE SUTC 1*, 186–193.

[24] MCCULLOCH, J., MCCARTHY, P., GURU, S., PENG, W., HUGO, D., AND TERHORST, A. 2008. Wireless sensor network deployment for water use efficiency in irrigation. In *Proceedings of the workshop on Real-world wireless sensor networks*. ACM New York, NY, USA, 46–50.

[25] MOTEIV. 2006. Tmote Sky datasheet. http://www.sentilla.com/pdf/eol/tmote-sky-datasheet.pdf.

[26] O'ROURKE, D., FEDOR, S., BRENNAN, C., AND COLLIER, M. 2007. Reception region characterisation using a 2.4 GHz direct sequence spread spectrum radio. In *Proceedings of the*

4th workshop on Embedded networked sensors (EmNets). ACM Press New York, NY, USA, 68–72.

[27] PORTER, J., ARZBERGER, P., BRAUN, H., BRYANT, P., GAGE, S., HANSEN, T., HANSON, P., LIN, C., LIN, F., KRATZ, T., MICHENER, W., SHAPIRO, S., WILLIAMS, T. 2005. Wireless Sensor Networks for Ecology. *BioScience 55*, 7, 561–572.

[28] RAMAN, B., CHEBROLU, K., MADABHUSHI, N., GOKHALE, D., VALIVETI, P., AND JAIN, D. 2006. Implications of link range and (In) stability on sensor network architecture. In *Proceedings of the 1st international workshop on Wireless network testbeds, experimental evaluation & characterization*. ACM New York, NY, USA, 65–72.

[29] RAPPAPORT, T. 2002. *Wireless Communications: Principles and Practice*. Prentice Hall.

[30] SOHRABI, K., MANRIQUEZ, B., AND POTTIE, G. 1999. Near ground wideband channel measurement in 800-1000 MHz. *Vehicular Technology Conference, 1999 IEEE 49th 1*.

[31] SUN, J. AND CARDELL-OLIVER, R. 2006. An experimental evaluation of temporal characteristics of communication links in outdoor sensor networks. In *Second ACM Workshop on Real-World Wireless Sensor Networks (REALWSN)*.

[32] THELEN, J., GOENSE, D., AND LANGENDOEN, K. 2005. Radio wave propagation in potato fields. In *1st Workshop on Wireless Network Measurements*. Riva del Garda, Italy.

[33] TI. 2006. TI CC2400 Datasheet. `http://www.ti.com/lit/gpn/cc2400`.

[34] TI. 2007. TI CC2420 Datasheet. `http://www.ti.com/lit/gpn/cc2420`.

[35] TI. 2008. TI E2E Community Forum message. `https://community.ti.com/forums/p/428/1139.aspx`.

[36] TOLLE, G., POLASTRE, J., SZEWCZYK, R., CULLER, D., TURNER, N., TU, K., BURGESS, S., DAWSON, T., BUONADONNA, P., GAY, D., HONG, W. 2005. A macroscope in the redwoods. In *Proceedings of the 3rd international conference on Embedded networked sensor systems*. ACM New York, NY, USA, 51–63.

[37] US DEPARTMENT OF AGRICULTURE. 2009. SNOTEL Data Collection Network Fact Sheet. `http://www.wcc.nrcs.usda.gov/factpub/sntlfct1.html`.

[38] US FOREST SERVICE. 2009. Remote Automated Weather Stations home page. `http://www.fs.fed.us/raws/`.

[39] VIEIRA, M., COELHO JR, C., DA SILVA JR, D., AND DA MATA, J. 2003. Survey on wireless sensor network devices. In *Emerging Technologies and Factory Automation, 2003. Proceedings. ETFA'03. IEEE Conference*. Vol. 1.

[40] WERNER-ALLEN, G., JOHNSON, J., RUIZ, M., LEES, J., AND WELSH, M. 2005. Monitoring volcanic eruptions with a wireless sensor network. In *Wireless Sensor Networks, 2005. Proceeedings of the Second European Workshop on*. 108–120.

[41] WHITMAN, E. 2005. SOSUS: The "secret weapon" of undersea surveillance. *Undersea Warfare 7*, 2 (Winter).

[42] WOOD, L. 1946. Automatic Weather Stations. *Journal of the Atmospheric Sciences 3*, 4, 115–121.

[43] WU, Y., SHI, C., ISMAIL, M., AND OLSSON, H. 2000. Temperature compensation design for a 2.4 GHz CMOS low noise amplifier. *Circuits and Systems, 2000. Proceedings. ISCAS 2000 Geneva. The 2000 IEEE International Symposium on 1*.

[44] YAMASHITA, S., SHIMURA, T., AIKI, K., ARA, K., OGATA, Y., SHIMOKAWA, I., TANAKA, T., KURIYAMA, H., SHIMADA, K., AND YANO, K. 2006. A 15x15 mm, 1uA, reliable sensornet module: enabling application-specific nodes. *Information Processing in Sensor Networks (IPSN)*.

[45] ZUNIGA, M. AND KRISHNAMACHARI, B. 2004. Analyzing the transitional region in low power wireless links. In *Sensor and Ad Hoc Communications and Networks, 2004. IEEE SECON 2004. 2004 First Annual IEEE Communications Society Conference on*. 517–526.

APPENDIX A

SOIL PROBE INTERFACE AND POWER CIRCUITRY

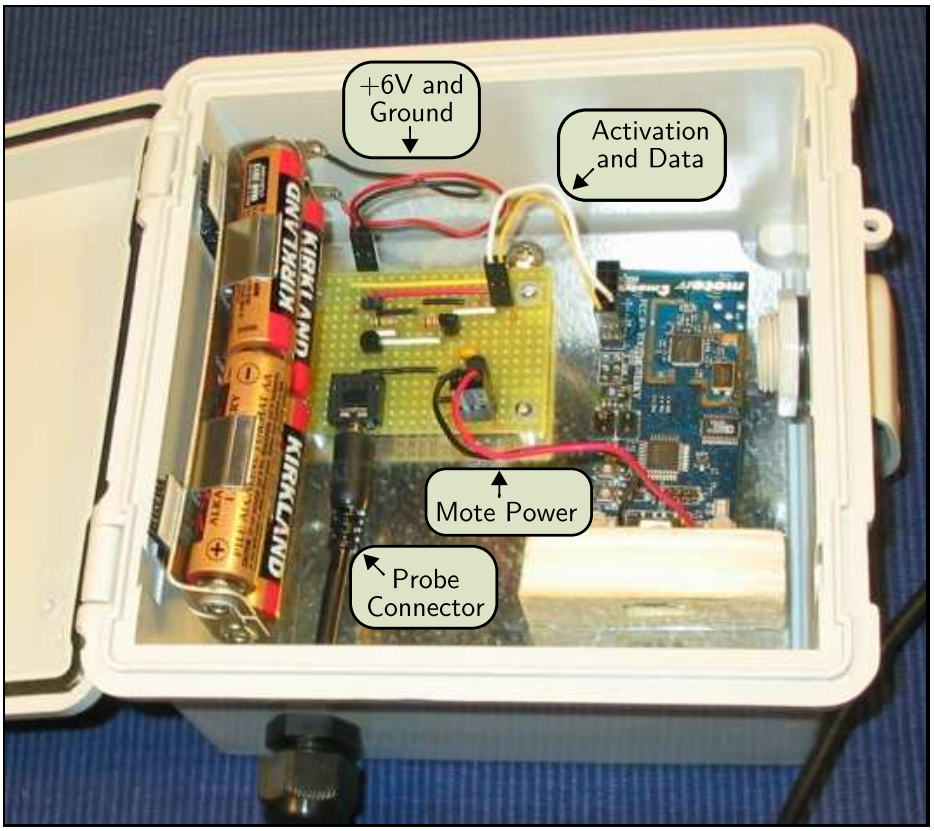

Figure 21. Enclosure containing Tmote Sky wireless module and interface circuitry

This chapter describes the hardware interface we developed to allow a TelosB-class mote to activate and collect data from a Decagon Devices ECH_2O-TE soil probe [7]. In addition the circuitry includes a voltage regulator to power the mote. Figure 21 shows the components in a weatherproof enclosure.

Essentially the interface between the probe and mote is an adapter between their requirements and limitations. The probe provides a three-pin stereo plug for excitation/power input, UART output, and ground. The probe requires 10 mA of current for 9 ms at 3.5 V or higher to power a sensor reading. Unfortunately the mote output pins only are capable of a maximum of 6 mA at 3.0 V; therefore the mote must trigger an external power source rather than providing the power itself. Data transfer is simple since the mote also supports UART communication.

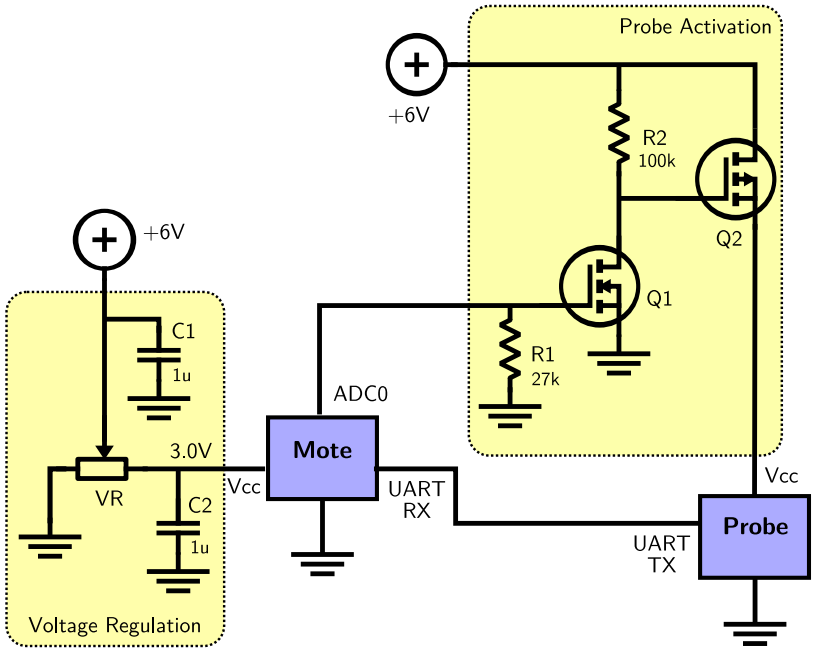

Figure 22. Schematic diagram of mote/probe interface and mote power source

We adapted a solution from [15], as shown in the Probe Activation portion of the schematic diagram in Figure 22. To activate the probe, the mote sets a general I/O pin, which switches on MOSFET Q1 (n-channel). This signal in turn switches MOSFET Q2 (p-channel), which then provides 6 V battery current to the probe. Two switches are required rather than just one to permit both the mote and the probe to use the common ground reference.

The power supply consists of four AA batteries to provide several months of power to the probe and the mote. As a consequence of the 6 V current level, a voltage regulator was required to provide an acceptable voltage level for the mote. This component and its supporting capacitors is shown in the Voltage Regulation section of Figure 22.

We also developed a TinyOS software driver for the hardware interface. The probe provides a reading to the driver in a digital format, as a sequence of ASCII characters over the UART interface. The driver in turn provides a standard TinyOS Read interface to the application. An application simply requests the read, and then the driver triggers the probe, uses the generic TinyOS

Table 4. Components used to implement the schematic in Figure 22

Code	Description
Q1	Supertex TN0606 3.0 V
Q2	Supertex TP0606 3.0 V
R1	27 kΩ, 1/4 W, 5%
R2	100 kΩ, 1/4 W, 5%
VR	Microchip MCP 1702, 3.0 V
C1, C2	1 μF ceramic

UART communication module to collect the values, and returns a structure containing the temperature, moisture, and conductivity values in physical units. The driver is freely available from the TinyOS user contributions repository [17].

APPENDIX B

SOURCE DATA, TOOLS, AND PROCEDURES

This chapter provides detailed descriptions of the tools and procedures used to collect and organize the data used in the body of the thesis. The descriptions are grouped by experiment. The data and some of the tools are available in an online archive as described in the text. The archive is located at `http://impact.asu.edu/thesis/bannister-archive.zip`.

Some tools use various free system utilities, including the Bash shell, Perl, awk, and MySQL.

1. Laboratory Signal Strength Measurements

We developed the mote software, procedures, and data post-processing tools for laboratory measurement of RSS. The files are located in the `lab_rss` directory of the archive. The list below describes the overall flow of activity from software development to data analysis with references to detailed information later in this section.

- Develop software. The software directs the motes to send test messages for RSS sampling as well as temperature readings, and then to output those readings for observation and storage. See the “Software” section below for more details.
- Run experimental trials. The software from the previous step was loaded onto the motes for the trials. The experimental setup and operation are detailed in “Experimental Procedures” below.
- Convert raw experimental data to useful values. First the raw, binary format data was converted to decimal values using the `splitdata` program in “Mote Software”. Then the individual data files were combined into Octave tables and comma separated values. See the `combine_data` program and listing of data files in “Trial Results” below.

1.1. Software. The source code to operate the motes is contained in the `src` subdirectory, with contents shown in the table below. As described in the thesis, the experimental procedure

differs slightly based on the location of the receiver mote: in the temperature chamber, or out at room temperature. The motes must be TelosB compatible. Our experiments used the Tmote Sky. The base TinyOS system was version 2.0, but the code should be compatible with later 2.x revisions.

`heat_base`	Mote source code for sender (Scout) and receiver (Base) when the receiver mote is heated.
`heat_scout`	Mote source code for sender (Scout) and receiver (Base) when the sender mote is heated.
`splitdata.pl`	PC-based script to post-process raw binary mote output into a columnar decimal format. Also useful as documentation for the raw binary format. The experimental trials use data format 50, which is the default format.
`splitdata.1`	Unix-style man page for `splitdata.pl`.
`README`	Details the contents of each subdirectory above.

1.2. Experimental Procedures. There are two procedures for running an experimental trial: one when the sender (Scout) is in the thermal chamber, and another when the receiver (Base) is in the chamber. The procedures are similar but differ in how the readings are collected.

When the sender is heated, readings are collected from the receiver (Base) mote:

1. Connect the USB cable from the base mote to the PC.
2. Start the serial forwarder and serial listener on the PC as shown in `base/serial-command`. Setup the listener to save its data to a file as it is generated. Then use a separate program to monitor the file contents in real time, such as the GNU tail program.
3. Send a START_RELAY command to the base unit, with output to UART. This directs output to the PC for observation.

4. Shortly thereafter the serial listener received Base noise readings every 60 seconds and weather readings every 30 seconds. Unfortunately the readings are output in raw hex format, which is difficult to use on the fly. The Perl script, `splitdata.pl`, described in ”Mote Software“ above, describes the format of the output.
5. Power up the Scout mote. The Scout then sends its burst of messages, followed by a weather reading at 20 second intervals.
6. This arrangement will continue to run until the motes are powered down. The temperature in the thermal chamber may be set as desired.

When the receiver is heated, readings are collected from the sender (Scout) mote. Internally the motes take readings at the same frequency as when the Scout mote is heated. However, the Base outputs all readings back over the radio to the Scout rather than outputting to UART or log. Although this procedure is slightly more complex internally, the operator procedure is a little simpler.

1. Connect the USB cable from the Scout mote to the PC.
2. Start the serial forwarder and serial listener on the PC as shown in `base/serial-command`. Setup the listener to save its data to a file as it is generated. Then use a separate program to monitor the file contents in real time, such as the GNU tail program.
3. Power up the Base mote. Shortly thereafter Base noise readings appear every 60 seconds and weather readings every 30 seconds from the serial listener. In addition the Scout’s weather readings appear every 20 seconds. Unfortunately the readings are output in raw hex format, which is difficult to use on the fly. The Perl script, `splitdata.pl`, described in ”Mote Software“ above, describes the format of the output.
4. This arrangement will continue to run until the motes are powered down. The temperature in the thermal chamber may be set as desired.

1.3. Trial Data. Four separate trials were run, and the results are contained in subdirectories in the table immediately below. The contents of each subdirectory are the same, and listed next.

Subdir	Date	Description
`recv_104`	2008-02-24	Mote 104 heated as receiver (Base)
`recv_106`	2008-02-22	Mote 106 heated as receiver (Base)
`xmit_104`	2008-02-23	Mote 104 heated as sender (Scout)
`xmit_106`	2008-02-21	Mote 106 heated as sender (Scout)

`noise.csv` Combined noise RSS and weather data (unused)

`noise.dat` Raw noise data sampled at receiver (unused)

`noise.mat` Combined noise RSS and weather data (unused)

`rssi_0dbm.csv` Combined RSS and weather data, one row per minute. Format: time (minutes), temperature (Celsius), RSS (dBm)

`rssi_0dbm.dat` Raw RSS data from receiver; sampled in a burst of 10 readings every 40 seconds. Format: sequence number, mean RSS (dBm), standard deviation, time (minutes)

`rssi_0dbm.mat` Combined RSS and weather data in Octave format.

`rssi_-15dbm.dat` Raw RSS data from receiver (unused)

`weather.dat` Raw weather (temperature) data from heated mote; sampled either every 20 seconds or 30 seconds. Format: sequence number, temperature (Celsius), relative humidity, time (minutes)

The top level `lab_data` directory contains two other files used to generate some of the trial data files:

`combine_data` Shell script to generate data files suitable for RSS and temperature analysis. Executes `combine_data.m` below as needed.

`combine_data.m` Octave script to process data files for a single subdirectory. The script combines RSS data in one file with weather (temperature) data in a second file to produce a single comma delimited data file. For example combines `rssi_0dbm.dat` and `weather.dat` to produce `rssi_0dbm.csv`. Raw data is averaged to produce a single row per minute.

2. Outdoor Signal Strength and Range Measurements

We developed the mote software, procedures, and data post-processing tools for outdoor measurement of RSS and communication range at Maricopa Agricultural Center. The files are located in the `mac` directory of the archive. Results in two sections of the thesis are derived from these results: Section 3.2 on the decrease in RSS with temperature when all packets received successfully; and Section 4.2 on the temperature for the maximum communication range over several distances.

As a top-level guide to the contents, the following outline describes how the data was generated, from mote development to final data tables. Details on each step are described in later sections of this document.

- Develop software. The software directs the motes to send test messages for RSS sampling as well as temperature readings, and then to output those readings for observation and storage. See the ”Software” section below for more details. Also see the conceptual documentation in the thesis itself.
- Run experimental trials. The software from the previous step was loaded onto the motes for the trials. Each trial included several hardware components described below. The experimental setup and operation are detailed in ”Experimental Procedure”.

- Six data collection motes, three fixed and three movable. Trials were performed at eight distances: from 26m to 40m inclusive every 2m. As the mote names indicate the fixed motes were stationary while the movable motes were relocated for each trial.
- Time beacon mote, which broadcast a sequence identifier every 45 seconds to keep the data collection motes synchronized.
- Base station mote attached to a PC. Used to send commands to motes for trial setup and monitoring.

◦ Convert raw experimental data to useful values. The data was converted from the mote's binary format to a text-based log format, and then to a columnar format, and finally to Octave matrices combining all data. The `motelisten` program described in the "Mote Software" section below was used to generate the raw log files from the mote binary data as it was downloaded over USB. For more information see the "Trial Results" section below.

2.1. Software. The source code to operate the hardware components, including the data collection motes themselves, is contained in the `src` subdirectory. All motes must be TelosB compatible. Our experiments used a Tmote Sky. The base TinyOS system was version 2.0, but the code should be compatible with later 2.x revisions.

`base-station`	Mote source code for the base station mote; essentially a router for messages to/from the data collection motes.
`motecmd`	PC source code to send/receive commands via the command line and serial port.
`rssmote`	Mote source code for the data collection motes.
`syncmote`	Mote source code for the time beacon mote.
`README`	Details the contents of each subdirectory above.

2.2. Experimental Procedures.

1. Set up PC and base station mote. The mote used a separate 9 dBi antenna mounted approx. 2m above ground to ensure reliable communication. The mote was located approximately 25 perpendicular meters from the axis between the fixed and movable motes.
2. Set up beacon mote. This mote use a separate 5 dBi antenna mounted on a tripod approx. 1m above ground to ensure reliable communication. The mote was located approximately 10 perpendicular meters from the axis between the fixed and movable motes.
3. Mount fixed/movable motes as needed, insert batteries, and cover with two white plastic kitchen garbage bags.
4. Send commands to fixed and movable motes to set up the trial. See the list of commands below this procedure.
5. Send command to beacon mote for beacon period (SET_SYNC_PERIOD 45s), and then start the beacon, which triggers the fixed and movable motes to execute the trial. For a description of the mote-level communication for data collection, see Section 3.2 in the thesis.
6. After approximately 24 hours, send command to beacon mote to stop beacon. Then collect each mote and download data via a USB connection.

Commands to set up fixed and mobile motes:

SET_RELAY_TARGETS	Set data output to Log
SET_???_SLOT	Identify mote as fixed (???=LEAD) or movable (???=RANGE) and the communication slot (1,2,3).
SET_SURVEY_PARAMS	Set output power to -10 dBm and survey period (135 for movable, 180 for fixed)
SET_OPMODE	Set to survey mode. Data collection will begin with next syncmote beacon received.

2.3. Trial Data. Data was converted from raw to useful values in a series of steps. The descriptions below are presented in reverse chronological order, which puts the final, most useful values first. The files are stored in the `data` subdirectory. The ultimate results is aggregation of all data into two files, which are described next.

`all_data.mat` – Octave matrix containing RSS and temperature data for test messages at each distance. Columns:

1. distance
2. RSS burst source mote ID
3. RSS burst target mote ID
4. elapsed time (s)
5. mean RSS
6. RSS standard deviation
7. packet reception rate
8. source mote temperature (C)
9. target mote temperature (C)
10. average mote temperature (C)

`noise_data.mat` – Octave matrix containing RSS and temperature data for sampled noise levels. Columns:

1. distance
2. noise RSS mote ID
3. elapsed time (s)
4. mean RSS
5. RSS standard deviation
6. mote temperature (C)

Within the `data` subdirectory are further subdirectories: `26`, `28`, `30`, `32`, `34`, `36`, `38`, and `40`; one for each of the eight trials at distances from 26 m to 40 m. Within each subdirectory is an identical collection of files which are the source for the Octave matrices described above. For each RSS burst source mote there are three text data files, one for each target. For example for mote 101 as an RSS source there are `m101-105.tbl`, `m101-200.tbl`, `m101-208.tbl`. Each file is a space-separated text file with columns:

1. elapsed time hours
2. elapsed time minutes
3. elapsed time seconds
4. mean RSS
5. RSS standard deviation
6. packet reception rate
7. source mote temperature (C)
8. target mote temperature (C)
9. average source/target mote temperature (C)

For each mote there also is one text file for RSS noise readings, for example

`m101-noise.tbl`, with columns:

1. elapsed time hours
2. elapsed time minutes
3. elapsed time seconds
4. mean RSS
5. RSS standard deviation
6. count of samples
7. mote temperature (C)

The conversion of these text files to the Octave matrices is accomplished by two Octave programs:

`import.m`	Imports `.tbl` text files to `all_data.mat`.
`import_noise.m`	Import noise `.tbl` text files to `noise_data.mat`.
`init_mac_globals.m`	Supporting data needed to execute import.

The `.tbl` text data files in turn were generated from the raw data collected by the motes, which is located in the `raw_data` subdirectory. Here again there is one further subdirectory for each distance, each containing six text log files, one for each mote. The data is in the form of a human-readable chronological log of all readings for the trial. For example the lines below describe reception of an RSS test message burst:

```
AM_SUM_RSS: current time 0:06:56, burst_num 5, src 105, tx_level 11,
mean RSS -88.3, SD 0.47, msg_count 100
```

Several script files are used to convert these log file entries into the columnar `.tbl` files in the `data` subdirectory:

`load_weather_data`	Loads temperature and humidity data into a MySQL table. The table allows random retrieval of temperature data, which is required to build the `.tbl` file.
`make_tables`	Top-level script to create columnar files from log files. Requires populated MySQL table created by `load_weather_data`. Places temperature readings from both source mote and target mote together with each RSS message burst reading in the `.tbl` file.
`weather.awk`	Support file required by `load_weather_data`.
`append_source_temp.pl`	Support file required by `make_tables` to append temperature data from MySQL database.
`noise-temp.awk`	Support file required by `make_tables`.

3. Data Collection Simulation

The data collection simulation was written using Matlab/Octave by Gianni Giorgetti, a research associate in the Impact Lab. Section 4.1 in the body of the thesis provides an overview of its operation. The data files generated from our experiments are located in the `sim` directory of the archive. The directory includes the data files from each of the 100 trials of the simulation and a summary data file. The structure of these files is described below.

`net_stats.mat` – Simulation state for each trial at each measured temperature. Temperatures vary from 20°C to 60°C at 5°C intervals. State includes:

1. Temperature (C)
2. Mean node connectivity for 1.0 PRR
3. Nodes connected to sink at 1.0 PRR(%)

4. Mean node connectivity for 0.4-1.0 PRR
5. Nodes connected to sink for 0.4+ PRR (%)
6. Mean ETX at 1.0 PRR
7. Mean ETX for 0.4+ PRR

`net_???.mat` – Per trial simulation data, where `???` in filename varies from 1 to 100. Contains `net`, the comprehensive Matlab/Octave data structure used by the simulation, which is described below. Values in the left column are the names of the data structure's attributes. Values in parentheses are the actual values for the simulation. For example (49x49) is a matrix with a column and a row for each node in the network grid.

Constant data across temperatures

`D`	Matrix of distance between each pair of points. (49x49)
`dim`	Number of dimensions for grid. (2)
`mult`	Length of each side of grid. (140)
`n`	Count of nodes in grid. (49)
`PL`	Matrix of path loss calculated from net.RSS. (49x49)
`pnoise`	Noise factor for grid placement, between 0 and 1. 0.2 means node position has a variance of 20% of true grid point.
`PTH`	Sensitivity threshhold (-94 dBm)
`radius`	1 (unused)
`RSS`	Matrix of calculated log-normal RSS for each pair. (49x49)
`RSS_P`	Vector of 3 values: path loss at unit distance (-39), path loss exponent (3.6), and path loss std dev (8.4)
`V`	n x 2 matrix of actual node (x,y) positions. (49,2)

Variable data; recalculated at each temperature increment

Recalculated by increasing the threshhold RSS for connectivity and then comparing with the values in net.RSS. For example from 30C to 35C the threshhold increased from approximately -92.2 dBm to -91.4 dBm. Several attributes appear in pairs where one attribute measures high quality links near 1.0 PRR and the second attribute, prefixed with `t_`, includes marginal links of 0.4 - 1.0 PRR. As stored in the data archive, the variable data contains the network state at the end of a trial, when temperature is 60C.

`A, t_A` Matrix of binary connectivity (0/1) between each pair of points. (49x49)

`conn` Calculated mean node connectivity at 1.0 PRR.

`conn_t` Calculated mean node connectivity at 0.4-1.0 PRR.

`etx` Matrix of estimated transmission count between all nodes (49x49). Thus the first row is hop count to sink node. Determined by the Floyd-Warshall algorithm.

`hc` Matrix of shortest path distance between all nodes (49x49). Thus the first row is hop count to sink node. Determined by the Floyd-Warshall algorithm.

`Nodes` Vector with an entry per node (49):

`ETX`: Vector of expected transmission count values to the nodes referenced by `t_NB`.

`NB, t_NB`: Vector of IDs of nodes connected to this node.

`nnb, t_nnb`: Count of connected nodes (size of NB).

`p`: Copy of coordinates of this node from net.V.

APPENDIX C

THESIS MATERIAL IN PREVIOUS PUBLICATIONS

Chapters 3 and 4 include material previously published in the conference paper, “Wireless Sensor Networking for ’Hot’ Applications: Effects of Temperature on Signal Strength, Data Collection and Localization” by Kenneth Bannister, Gianni Giorgetti, and Sandeep K.S. Gupta, which appeared in *Proceedings of the Fifth Workshop on Embedded Networked Sensors*, Charlottesville, VA, June 2008.